JACS
JOURNAL OF THE AMERICAN CHEMICAL SOCIETY

ARTICLE

pubs.acs.org/JACS

Supported-Nanoparticle Heterogeneous Catalyst Formation in Contact with Solution: Kinetics and Proposed Mechanism for the Conversion of Ir(1,5-COD)Cl/γ-Al_2O_3 to Ir(0)$_{\sim 900}$/γ-Al_2O_3

Joseph E. Mondloch and Richard G. Finke*

Department of Chemistry, Colorado State University, Fort Collins, Colorado 80523, United States

Supporting Information

ABSTRACT: A current goal in heterogeneous catalysis is to transfer the synthetic, as well as developing mechanistic, insights from the modern revolution in nanoparticle science to the synthesis of supported-nanoparticle heterogeneous catalysts. In a recent study (Mondloch, J. E.; Wang, Q.; Frenkel, A. I.; Finke, R. G. *J. Am. Chem. Soc.* **2010**, *132*, 9701−9714), we initialized tests of the global hypothesis that quantitative kinetic and mechanistic studies, of supported-nanoparticle heterogeneous catalyst formation *in contact with solution*, can provide synthetic and mechanistic insights that can eventually drive improved syntheses of composition-, size-, and possibly shape-controlled catalysts. That study relied on the development of a well-characterized Ir(1,5-COD)Cl/γ-Al_2O_3 precatalyst, which, when in contact with solution and H_2, turns into a nonaggregated Ir(0)$_{\sim 900}$/γ-Al_2O_3 supported-nanoparticle heterogeneous catalyst. The kinetics of the Ir(1,5-COD)Cl/γ-Al_2O_3 to Ir(0)$_{\sim 900}$/γ-Al_2O_3 conversion were followed and fit by a two-step mechanism consisting of nucleation (A → B, rate constant k_1) followed by autocatalytic surface growth (A + B → 2B, rate constant k_2). *However, a crucial, but previously unanswered question is whether the nucleation and growth steps occur primarily in solution, on the support, or possibly in both phases for one or more of the catalyst-formation steps.* The present work investigates this central question for the prototype Ir(1,5-COD)Cl/γ-Al_2O_3 to Ir(0)$_{\sim 900}$/γ-Al_2O_3 system. Solvent variation-, γ-Al_2O_3-, and acetone-dependent kinetic data, along with UV−vis spectroscopic and gas−liquid-chromatography (GLC) data, are consistent with and strongly supportive of a supported-nanoparticle formation mechanism consisting of Ir(1,5-COD)Cl(solvent) dissociation from the γ-Al_2O_3 support (i.e., from Ir(1,5-COD)Cl/γ-Al_2O_3), solution-based nucleation from that dissociated Ir(1,5-COD)Cl(solvent) species, fast Ir(0)$_n$ nanoparticle capture by γ-Al_2O_3, and then subsequent solid-oxide-based nanoparticle growth from Ir(0)$_n$/γ-Al_2O_3 and with Ir(1,5-COD)Cl(solvent), the first kinetically documented mechanism of this type. Those data disprove a solid-oxide-based nucleation and growth pathway involving only Ir(1,5-COD)Cl/γ-Al_2O_3 and also disprove a solution-based nanoparticle growth pathway involving Ir(1,5-COD)Cl(solvent) and Ir(0)$_n$ in solution. The present mechanistic studies allow comparisons of the Ir(1,5-COD)Cl/γ-Al_2O_3 to Ir(0)$_{\sim 900}$/γ-Al_2O_3 supported-nanoparticle formation system to the kinetically and mechanistically well-studied, Ir(1,5-COD)·$P_2W_{15}Nb_3O_{62}^{8-}$ to Ir(0)$_{\sim 300}$·$(P_2W_{15}Nb_3O_{62}^{8-})_n^{-8n}$ solution-based, polyoxoanion-stabilized nanoparticle formation and stabilization system. That comparison reveals closely analogous, solution Ir(1,5-COD)$^+$ or Ir(1,5-COD)Cl-mediated, mechanisms of nanoparticle formation. Overall, the hypothesis supported by this work is that these and analogous studies hold promise of providing a way to transfer the synthetic and mechanistic insights, from the modern revolution in nanoparticle synthesis and characterization in solution, to the rational, mechanism-directed syntheses of solid oxide-supported nanoparticle heterogeneous catalysts, also in contact with solution.

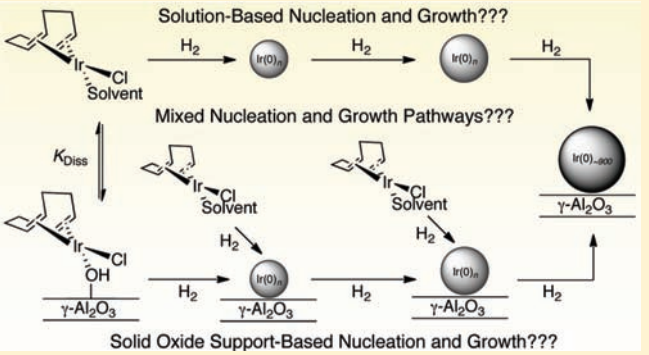

INTRODUCTION

Small metal nanoparticles supported on metal-oxide supports constitute a large, important subset of heterogeneous catalysts.[1] Despite their importance, the synthesis of these industrially significant catalysts is still largely empirical.[2] Hence, a current goal in catalyst preparation is to transfer the synthetic,[3] as well as developing mechanistic,[4−10] insights from the modern revolution in nanoparticle science, including control over nanoparticle composition,[11] size,[12] and shape,[13] to the synthesis of supported-nanoparticle heterogeneous catalysts.[14] However, despite the now considerable insights into the synthesis, characterization, and mechanisms of formation of nanoparticles in solution, transferring that synthetic and mechanistic knowledge to the preparation of supported heterogeneous catalysts remains largely unaccomplished, if not elusive.

Received: November 23, 2010
Published: April 28, 2011

At present, a common approach to preparing supported-nanoparticle catalysts is to first make the nanoparticles in solution (often with polymer or other ligands as stabilizers to prevent aggregation[15,16]), isolate the nanoparticles, and then deposit those ligand-stabilized nanoparticles onto a support.[15,16] Unfortunately, the polymer or other stabilizers are thereby unavoidably codeposited. Complete removal of the stabilizing polymer or other ligands has proven difficult to impossible[15,16] (such ligand removal being required for the most facile, coordinatively unsaturated catalysts). The resultant, partially ligand- or polymer-poisoned, supported-nanoparticles are then, and in turn, also compositionally ill-defined. That poorly defined composition as well as their size and shape are often then further altered by harsh thermal, oxidative, reductive, or other treatments aimed at removing the poisoning ligands or polymers.[16]

A more attractive, alternative synthetic approach, one that dates in part back to at least 1982[18a] and which is now attracting increasing attention,[14,17,18] is to start from supported molecular precursors and then synthesize the supported-nanoparticles in situ (i.e., in contact with solution) and *with only the desired catalytic reaction substrates or other ligands present*. At least in principle, this in situ method can provide additional control over the supported-nanoparticle composition, size, and shape, because one can readily add desired solvents, ligands, or other additives at will during the synthesis. Having only the desired reactants or other weakly bound ligands present can lead to what we have termed "weakly ligated/labile ligand" nanoparticles.[19,20]

Another potential advantage of the in situ, solution-based method is the ability to follow directly the supported-nanoparticle heterogeneous catalyst formation kinetics.[14,17] Kinetic and mechanistic studies are expected to be significant because key catalytic properties,[21] including selectivity,[22] activity,[21] lifetime, and stability,[23] depend on the nanoparticle catalyst surface composition,[24] size,[25] and structure. These properties are in turn dependent on the kinetics and mechanism(s) of nanoparticle formation (i.e., minimally nanoparticle nucleation and growth),[22] plus the specific solvent and ligands present.

Only six prior studies have addressed the mechanisms of supported-nanoparticle heterogeneous catalyst formation in contact with solution.[14,17,26−29] Of those six studies, only two[14,17] have provided kinetic data consistent with their proposed mechanisms, a point confirmed by our recent review[30] of the surprisingly limited number of prior studies examining the kinetics and mechanisms of practical heterogeneous catalyst formation under any conditions. Furthermore, no prior study begins from a fully characterized, speciation-controlled organometallic precatalyst[14,31] where the supported-nanoparticle stoichiometry is established[14] and where the kinetics of the supported-nanoparticle formation are also followed.[14] Nor has any of the solvent variation-, γ-Al_2O_3-, or acetone-dependent kinetic data given herein been previously reported for any prior system.

The Prototype Ir(1,5-COD)Cl/γ-Al_2O_3 to Ir(0)$_{\sim 900}$/γ-Al_2O_3 System. Recently, we reported the development of the Ir(1,5-COD)Cl/γ-Al_2O_3 to Ir(0)$_{\sim 900}$/γ-Al_2O_3 supported-nanoparticle heterogeneous catalyst formation system in contact with just acetone solvent plus the catalytic reactants cyclohexene and H_2, Scheme 1.[14] Crucial to the kinetic and mechanistic studies presented herein, the speciation-controlled Ir(1,5-COD)Cl/γ-Al_2O_3 precatalyst (Scheme 1, left; a single supported species) was fully characterized via inductively coupled optical emission spectroscopy, CO/IR trapping experiments, as well as X-ray absorbance fine structure spectroscopy (XAFS).[14] A balanced stoichiometry for the conversion of the Ir(1,5-COD)Cl/γ-Al_2O_3 precatalyst into the supported-nanoparticle product (Scheme 1, right) was also obtained along with characterization of the resultant Ir(0)$_{\sim 900}$/γ-Al_2O_3 catalyst by transmission electron microscopy (TEM) and XAFS. The results reveal nonaggregated, near-monodisperse (i.e., $\leq \pm 15\%$) 2.9 $\pm$ 0.4 nm nanoparticles supported on γ-Al_2O_3 (i.e., Ir(0)$_{\sim 900}$/γ-Al_2O_3).[14] Such a well-characterized, speciation-controlled Ir(1,5-COD)Cl/γ-Al_2O_3 precatalyst and resultant near-monodisperse Ir(0)$_{\sim 900}$/γ-Al_2O_3 catalyst are important prior results[14] that underpin the present studies. The eight criteria previously developed as the working definition of a prototype supported-nanoparticle heterogeneous catalyst formation system in contact with solution are detailed in a footnote for the interested reader.[32]

Initial kinetic studies, followed by the precedented[4−8,14,17] cyclohexene reporter reaction method (Scheme 2, left), were also performed as part of our prior work[14] and revealed that the supported-nanoparticle heterogeneous catalyst formation kinetics (Figure 1) are well fit to a two-step mechanism of nucleation (A $\rightarrow$ B, rate constant k_{1obs}) followed by autocatalytic surface growth (A + B $\rightarrow$ 2B, rate constant k_{2obs}), Scheme 2 (right). However, a crucial but until now unanswered question is whether nucleation and growth take place (i) homogeneously in solution, (ii) heterogeneously on the support, or conceivably (iii) in both phases for one or more of the catalyst formation steps. It is the answer to these questions that is the focal point of the present study.

Scheme 1. The Recently Developed[14] Ir(1,5-COD)Cl/γ-Al_2O_3 (Left) to Ir(0)$_{\sim 900}$/γ-Al_2O_3 (Right, TEM Imaging) Supported-Nanoparticle Heterogeneous Catalyst Formation System in Contact with Solution

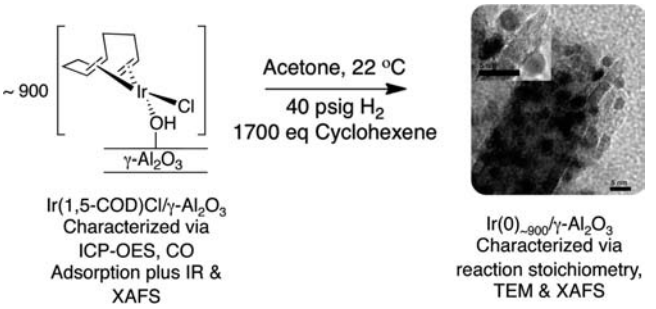

Scheme 2. The Cyclohexene Reporter Reaction Method Used To Follow the Supported-Nanoparticle Heterogeneous Catalyst Formation Kinetics (Left), Along with the Two-Step Mechanism That Has Been Shown to[14] Fit the Overall Ir(1,5-COD)Cl/γ-Al_2O_3 to Ir(0)$_{\sim 900}$/γ-Al_2O_3 Supported-Nanoparticle Formation Kinetics (Right)

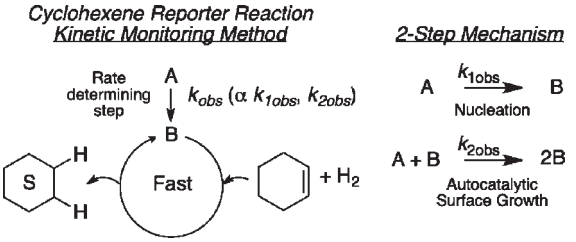

dx.doi.org/10.1021/ja110550h | J. Am. Chem. Soc. 2011, 133, 7744–7756

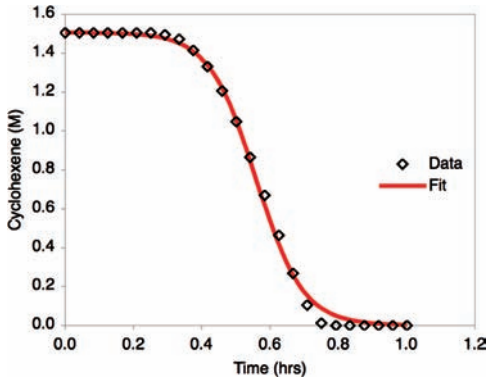

Figure 1. Sigmoidal kinetics previously observed[14] for Ir(1,5-COD)Cl/γ-Al_2O_3 to Ir(0)$_{\sim 900}$/γ-Al_2O_3 supported-nanoparticle heterogeneous catalyst formation (◇) using the cyclohexene reporter reaction method (Scheme 2), plus the subsequent curve-fit to the two-step, A → B (rate constant, k_1), A + B → 2B (rate constant, k_2) mechanism for nanoparticle formation (red line).[14] The experimental error bars for the k_1 and k_2 values are reported in Table 1, vide infra.

Herein, we present kinetic and mechanistic studies probing precisely in which phase (or phases; solution, solid-state, or both) the nucleation and growth catalyst formation steps occur for the Ir(1,5-COD)Cl/γ-Al_2O_3 to Ir(0)$_{\sim 900}$/γ-Al_2O_3 system while in contact with acetone or acetone/cyclohexane solution. Solvent variation-, γ-Al_2O_3-, and acetone-dependent kinetic data (as well as UV−vis spectroscopic and GLC data) offer evidence consistent with and strongly supportive of Ir(1,5-COD)Cl(solvent) solution-based nucleation, fast Ir(0)$_n$ nanoparticle capture by γ-Al_2O_3, and solid-oxide-based supported-nanoparticle growth from that Ir(0)$_n$/γ-Al_2O_3 with Ir(1,5-COD)Cl(solvent). This proposed mechanism is also consistent with our prior product studies,[14] the observation of nonaggregated 2.9 ± 0.4 nm supported Ir(0)$_n$ nanoparticles on γ-Al_2O_3. Importantly, the data also disprove a Ir(1,5-COD)Cl/γ-Al_2O_3 solid-oxide-based nucleation and growth mechanism as well as a solution-based nanoparticle growth pathway. We have also been able to make the first comparisons between the present Ir(1,5-COD)Cl/γ-Al_2O_3 to Ir(0)$_{\sim 900}$/γ-Al_2O_3 nanoparticle formation system and the previously well-studied, polyoxoanion-supported/stabilized Ir(1,5-COD)·$P_2W_{15}Nb_3O_{62}^{8-}$ to Ir(0)$_{\sim 300}$·$(P_2W_{15}Nb_3O_{62}^{8-})_n^{-8n}$ nanoparticle formation and stabilization system. Intriguingly, that first-of-its kind comparison reveals that both systems exhibit a Ir(1,5-COD)$^+$ dissociative, solution-based mechanism of nanoparticle catalyst formation. Overall, the results presented herein support the global hypothesis underlying the present work, namely that quantitative kinetic and mechanistic studies, of the formation of well-defined supported-nanoparticle heterogeneous catalysts from supported-organometallic precatalysts such as Ir(1,5-COD)Cl/γ-Al_2O_3 while in contact with solution, will yield insights into this potentially important, but to-date relatively little[14,17,26−29] investigated, alternative method of heterogeneous catalyst synthesis.

RESULTS AND DISCUSSION

Demonstration of Highly Solvent-Dependent Nucleation and Growth Kinetics Starting from Ir(1,5-COD)Cl/γ-Al_2O_3. To start, four solvents were surveyed including our standard solvent for nanoparticle formation, acetone,[14] to see how such solvent changes would affect the observed supported-nanoparticle heterogeneous catalyst formation kinetics. Solution-based, "homogeneous" nanoparticle nucleation and growth pathways are expected to be especially sensitive to solvent coordination/ligation ability.

Table 1. Kinetic Data for the Formation of Ir(0)$_n$/γ-Al_2O_3 from Ir(1,5-COD)Cl/γ-Al_2O_3 in the Four Solvents Surveyed

solvent	k_{1obs} (h^{-1})[a]	k_{2obs} (h^{-1} M^{-1})[a,b]
acetone	$1.5(1.1) \times 10^{-3}$	$1.6(2) \times 10^{4}$
propylene carbonate	$2.2(8) \times 10^{-4}$	$2.1(2) \times 10^{3}$
CH_2Cl_2	$5(4) \times 10^{-7}$	$2.4(2) \times 10^{3}$
cyclohexane	$8(6) \times 10^{-5}$	$2.2(5) \times 10^{2}$

[a] Each entry is the average (and standard deviation) of at least three separate supported-nanoparticle heterogeneous catalyst formation reactions under otherwise identical conditions. Specifically, 0.05 g of the 2.0 wt % Ir(1,5-COD)Cl/γ-Al_2O_3 precatalyst was suspended in 2.5 mL of solvent, 0.5 mL of cyclohexene, and reduced under 40 psig of H_2 while being stirred at 600 rpm. [b] The k_{2obs} values were corrected by the mathematically required stoichiometry factor of ∼1700 as detailed elsewhere.[30] That stoichiometry factor simply reflects the 1700:1 (Ir(1,5-COD)Cl/γ-Al_2O_3:cyclohexene) ratio employed in the reporter reaction, Scheme 2.[14]

The solvents chosen were based primarily on our prior Ir(0)$_n$-nanoparticle formation and stabilization studies,[33,34b] as well as their anticipated ability to coordinate (or not) to the supported Ir(1,5-COD)Cl moiety to yield dissociated Ir(1,5-COD)Cl(solvent). Table 1 summarizes the results of the kinetic experiments in the four solvents (the kinetic curves, plus their fits to the two-step mechanism, are provided in the Supporting Information). The data demonstrate rather clearly that the more coordinating solvent acetone exhibits facile nucleation and growth kinetics, while more weakly coordinating solvents such as propylene carbonate, CH_2Cl_2, and cyclohexane have much slower nucleation (k_{1obs}) and autocatalytic surface-growth (k_{2obs}) kinetics. Quantitatively, k_{1obs} varies by ∼3000-fold and k_{2obs} by ∼70-fold over the range of the four solvents examined. In short, the solvent is exhibiting a large effect on especially the observed nucleation kinetics, data suggestive of a kinetically important, if not dominant, solution-based component in the underlying mechanism.

For what follows, we have found it best for the typical reader if we present first the proposed mechanism, the evidence for that mechanism, and finally the alternative mechanisms that have been ruled out en route to the proposed mechanism. The mechanistic work itself of course proceeded in the opposite order historically, with the alternative mechanisms being disproved over more than a year period before we arrived at the proposed mechanism that follows.

The Proposed Mechanism: Ir(1,5-COD)Cl(solvent) Solution-Based Nucleation, Fast Nanoparticle Capture by [γ-Al_2O_3]$_{sus}$, and Subsequent Solid-Oxide-Based Supported-Nanoparticle Growth via Ir(1,5-COD)Cl(solvent) Plus Ir(0)$_n$/γ-Al_2O_3. The proposed mechanism in Scheme 3 (bold) begins with a dissociative equilibrium (K_{Diss}) between Ir(1,5-COD)Cl/γ-Al_2O_3 and Ir(1,5-COD)Cl(solvent) (abbreviated [Ir^I/Al_2O_3]$_{sus}$ and [Ir^I*solvent] in eqs 1−4, respectively). Nucleation in Scheme 3 is proposed to occur from the dissociated "homogeneous" Ir(1,5-COD)Cl(solvent) complex in solution (k_1'), followed by fast nanoparticle capture by [γ-Al_2O_3]$_{sus}$ (consistent with the observation of the unaggregated, 2.9 ± 0.4 nm supported Ir(0)$_n$

dx.doi.org/10.1021/ja110550h |J. Am. Chem. Soc. 2011, 133, 7744–7756

Scheme 3. The Proposed Supported-Nanoparticle Heterogeneous Catalyst Formation Mechanism (Bold) Involving Ir(1,5-COD)Cl(Solvent) Solution-Based Nucleation, Fast $Ir(0)_n$ Nanoparticle Capture by $[\gamma\text{-}Al_2O_3]_{sus}$, and Subsequent Solid-Oxide-Based Nanoparticle Growth between $Ir(0)_n/\gamma\text{-}Al_2O_3$ and Ir(1,5-COD)Cl(Solvent)[a]

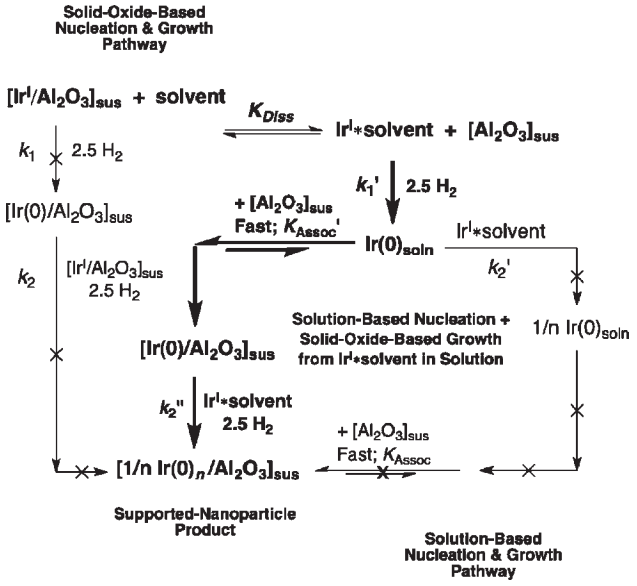

[a] Also shown are two alternative supported-nanoparticle heterogeneous catalyst formation mechanisms that were disproved (vide infra, the pathways crossed out).

nanoparticles). Subsequently, "heterogeneous", solid-oxide-based $Ir(0)_n/\gamma\text{-}Al_2O_3$ nanoparticle growth is then proposed to occur between $Ir(0)_n/\gamma\text{-}Al_2O_3$ and the dissociated Ir(1,5-COD)Cl(solvent) complex.

In the associated kinetic expressions provided next (the full derivations for which are provided in the Supporting Information), the Ir(1,5-COD)Cl/$\gamma\text{-}Al_2O_3$ precatalyst and $\gamma\text{-}Al_2O_3$ (abbreviated $[Al_2O_3]_{sus}$) have necessarily been approximated as being "homogeneously suspended in solution", as indicated by the "sus" subscripts (for suspended) in Scheme 3. That is, the hypothetical "concentrations" of active "Ir(1,5-COD)Cl" binding sites of the suspended $[\gamma\text{-}Al_2O_3]_{sus}$ are treated as if they increase linearly when in contact with solution (or, really, with the amount of solvent-exposed $[\gamma\text{-}Al_2O_3]$ surface area). As we will see, this necessary assumption is justified ex post facto by the results obtained.

In terms of evidence supporting the proposed mechanism, to start the Ir(1,5-COD)Cl/$\gamma\text{-}Al_2O_3$ to $Ir(0)_n/\gamma\text{-}Al_2O_3$ supported-nanoparticle heterogeneous catalyst formation kinetics are quantitatively accounted for (fit) by the two-step mechanism shown in Scheme 2 (e.g., from Figure 1), that is, by A → B and A + B → 2B (k_{obs}, Scheme 2).[14] Therefore, we can begin the needed kinetic derivations associated with Scheme 3 by writing the rate equation for the two-step mechanism, but now with solution-based nucleation from Ir(1,5-COD)Cl(solvent), fast $Ir(0)_n$ nanoparticle capture by $[\gamma\text{-}Al_2O_3]_{sus}$, and then solid-oxide-based nanoparticle growth (i.e., k_1' and k_2''), eq 1, and all as shown in Scheme 3.

$$-\frac{d[Ir^I/Al_2O_3]_{sus}}{dt} = k_1'[Ir^I{*}solvent]_t + k_2''[Ir^I{*}solvent]_t[Ir(0)_n/Al_2O_3]_{sus,t} \quad (1)$$

In eq 1 and the equations that follow, the subscript "i" represents initial concentrations, while the subscript "t" denotes each species as a function of time. Next, we express eq 1 in terms of the $[Ir^I/Al_2O_3]_{sus,i}$ that we experimentally begin with (i.e., what we measure out). Solving eq 2 for $[Ir^I{*}solvent]_t$, followed by subsequent substitution into the mass balance equation, eq 3, are straightforward, but key, steps in the complete derivation provided in the Supporting Information.

$$K_{Diss} = \frac{[Ir^I{*}solvent]_t[Al_2O_3]_{sus,t}}{[Ir^I/Al_2O_3]_{sus,t}[solvent]_t} \quad (2)$$

$$[Ir^I/Al_2O_3]_{sus,i} = [Ir^I/Al_2O_3]_{sus,t} + [Ir^I{*}solvent]_t \quad (3)$$

Substitution of the resultant $[Ir^I/Al_2O_3]_{sus,t}$ equation back into eq 1 yields the relevant rate equation for Scheme 3, eq 4, where the resultant k_{1obs} and k_{2obs} rate constants are given by eqs 5 and 6, respectively.

$$-\frac{d[A/Al_2O_3]_{sus}}{dt} = k_{1obs}[Ir^I/Al_2O_3]_{sus,i} + k_{2obs}[Ir^I/Al_2O_3]_{sus,i}[Ir(0)_n/Al_2O_3]_{sus,t} \quad (4)$$

$$k_{1obs} = \frac{k_1'K_{Diss}[solvent]_t}{[Al_2O_3]_{sus,t} + K_{Diss}[solvent]_t} \quad (5)$$

$$k_{2obs} = \frac{k_2''K_{Diss}[solvent]_t}{[Al_2O_3]_{sus,t} + K_{Diss}[solvent]_t} \quad (6)$$

The mechanism in Scheme 3 (bold), along with eqs 5 and 6, predicts that both $[\gamma\text{-}Al_2O_3]_{sus}$ and [solvent] will directly influence k_{1obs} and k_{2obs}, as makes sense conceptually based on the K_{Diss} equilibrium and its $[\gamma\text{-}Al_2O_3]_{sus}$ and [solvent] terms shown in Scheme 3.

Effects of $[\gamma\text{-}Al_2O_3]_{sus}$ on k_{2obs} and k_{1obs} Starting from Ir(1,5-COD)Cl/$\gamma\text{-}Al_2O_3$: Evidence Consistent with and Strongly Supportive of the Proposed Mechanism in Scheme 3. To test the predictions of the mechanism in Scheme 3, we started by varying the amount of well-stirred, suspended $\gamma\text{-}Al_2O_3$ in acetone, $[\gamma\text{-}Al_2O_3]_{sus}$, from 0.25 to 0.98 M.[35] In each case, the observed kinetics were sigmoidal and well-fit to the two-step mechanism, data further consistent with and supportive of the two-step nucleation and growth mechanism employed in the underlying derivation of eqs 5 and 6.

We looked first at the k_{2obs} (nanoparticle growth) versus $[\gamma\text{-}Al_2O_3]_{sus}$ dependence data as our prior experience as well as a a multitude of literature[36] show that the inherent error in nucleation rate constants (i.e., k_{1obs}) are large (up to $10^{\pm 1.2}$ in even the best behaved systems, for example[36]). Restated, our expectation was that the typical nucleation rate constant error bars would likely prohibit quantification of the k_{1obs} versus $[\gamma\text{-}Al_2O_3]_{sus}$ data, so we focused, instead, on the k_{2obs} versus $[\gamma\text{-}Al_2O_3]_{sus}$ data to start.

The extracted k_{2obs} values are plotted versus the $[\gamma\text{-}Al_2O_3]_{sus}$, Figure 2, black circles.[37] Qualitatively, k_{2obs} decreases with increasing $[\gamma\text{-}Al_2O_3]_{sus}$ as predicted by the mechanism in Scheme 3 and its associated equations, eq 6. This expected trend is due to the increased $[\gamma\text{-}Al_2O_3]_{sus}$ shifting the K_{Diss} equilibrium in Scheme 3 to the left, resulting in less Ir(1,5-COD)Cl(solvent) in solution, with a subsequent concomitant decrease in k_{2obs}. Significantly, we were also able to confirm, via UV−vis spectroscopy, that there

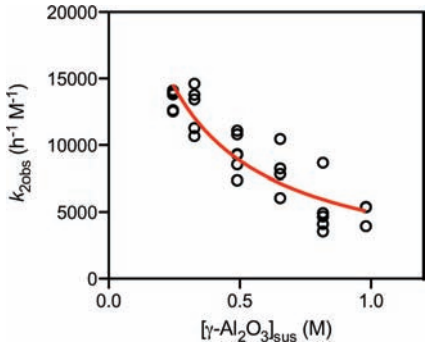

Figure 2. Dependence of the k_{2obs} rate constant on [γ-Al_2O_3]$_{sus}$, ○. The red line is the weighted nonlinear least-squares fit to eq 6 derived for the proposed mechanism (the bold pathway) in Scheme 3. The resultant K_{Diss} and k_2' values are 1.3(6) × 10^{-2} and 4(1) × 10^4 h^{-1} M^{-1}, respectively.

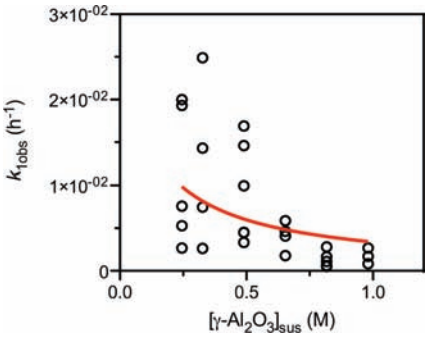

Figure 3. Dependence of the k_{1obs} rate constant on [γ-Al_2O_3]$_{sus}$, ○. The red line is the weighted nonlinear least-squares fit to eq 5 obtained by constraining the K_{Diss} equilibrium to 0.013, yielding a value for k_1' = 2.6(4) × 10^{-2} h^{-1}.

is in fact less Ir(1,5-COD)Cl(solvent) in solution with increasing [γ-Al_2O_3]$_{sus}$, data that are nicely accounted for by the K_{Diss} equilibrium in Scheme 3 (see the Supporting Information, Figure S2). In short, the combined kinetic and spectroscopic results are consistent with Ir(1,5-COD)Cl(solvent) being a kinetically dominant intermediate en route to Ir(0)$_n$/γ-Al_2O_3.

Quantitatively, using weighted nonlinear least-squares analysis (as detailed in the Experimental Section), eq 6 was found to provide a good fit to the [γ-Al_2O_3]$_{sus}$-dependent k_{2obs} data, Figure 2 (red line), yielding values of k_2'' = 4(1) × 10^4 h^{-1} M^{-1} and K_{Diss} = 1.3(6) × 10^{-2}. In addition, independent verification of the K_{Diss} equilibrium was obtained in a control experiment using gas−liquid chromatography (GLC). This was done by filtering off the solution from the (equilibrated) Ir(1,5-COD)Cl/γ-Al_2O_3 plus acetone solution, then hydrogenating the Ir(1,5-COD)Cl(solvent) complex and quantifying the amount of cyclooctane released in solution (i.e., as a marker for the amount of Ir(1,5-COD)Cl(solvent) present in solution). Pleasingly, the independently determined K_{Diss} equilibrium value (via GLC) was found to be K_{Diss} = 1.1 × 10^{-2}, the same within experimental error as the k_{2obs} versus [γ-Al_2O_3]$_{sus}$ fit-determined K_{Diss} value, K_{Diss} = 1.3(6) × 10^{-2}. The quantitative agreement between the kinetic- vs GLC-obtained K_{Diss} values provides very strong if not compelling support for (i) the mechanism in Scheme 3, (ii) the assumptions necessary in the derivation of the associated kinetic equations (e.g., that the γ-Al_2O_3 behaves as if it were "homogeneously suspended" with a "concentration", [γ-Al_2O_3]$_{sus}$, of Ir(1,5-COD)Cl binding sites), and (iii) also the kinetic and GLC experiments, analyses, and resultant data. The results yield the first experimental determination of such a K_{Diss}[30] equilibrium for supported-nanoparticle heterogeneous catalyst formation in contact with solution.

Returning to the observed nucleation rate constant data, we were encouraged to see if the extracted k_{1obs} values might not at least show the expected trend versus the [γ-Al_2O_3]$_{sus}$, and despite the always observed large errors in such nucleation rate constants.[36] The resultant k_{1obs} versus the [γ-Al_2O_3]$_{sus}$ plot is shown in Figure 3, ○.[37] Again pleasingly and fully consistent with eq 5 derived from Scheme 3, k_{1obs} does indeed show an [γ-Al_2O_3]$_{sus}$ dependency in the "correct direction". That is, qualitatively, k_{1obs} decreases with increasing [γ-Al_2O_3]$_{sus}$ as expected if nucleation is occurring from the dissociated, Ir(1,5-COD)Cl(solvent) complex in solution, Scheme 3, and its K_{Diss} equilibrium. There is the expected large scatter[36] in k_{1obs} for the 28 experimental data points plotted in Figure 3; not unexpectedly, weighted nonlinear least-squares curve-fitting using eq 5 did not converge on k_1' and K_{Diss} values. However, constraining the K_{Diss} to its known value of 0.013, eq 5 was able to at least qualitatively account for the rough shape of the k_{1obs} versus [γ-Al_2O_3]$_{sus}$ data, Figure 3 (red line), resulting in a value of k_1' = 2.6(4) × 10^{-2} h^{-1}. While the k_{1obs} versus [γ-Al_2O_3]$_{sus}$ data are noisy as expected,[36] the results are still consistent with the proposed mechanism in Scheme 3.

Overall, the k_{2obs} and k_{1obs} versus [γ-Al_2O_3]$_{sus}$ kinetic data, the independent verification of the K_{Diss} equilibrium via GLC, and the decrease in Ir(1,5-COD)Cl(solvent) with increasing [γ-Al_2O_3]$_{sus}$ (monitored via UV−vis spectroscopy) are all highly consistent with and strongly supportive of the mechanism in Scheme 3: Ir(1,5-COD)Cl(solvent) dissociation followed by solution-based nucleation, fast Ir(0)$_n$ nanoparticle capture by [γ-Al_2O_3]$_{sus}$, and then subsequent nanoparticle growth from the solid-oxide-supported Ir(0)$_n$/γ-Al_2O_3 plus the dissociated Ir(1,5-COD)Cl(solvent) complex.

Effects of [Acetone] on k_{2obs} and k_{1obs} Starting from Ir(1,5-COD)Cl/γ-Al_2O_3: Further Evidence Consistent with the Proposed Mechanism in Scheme 3. Equations 5 and 6 derived from the mechanism in Scheme 3 predict that both k_{2obs} and k_{1obs} should also depend on the "solvent" concentration. Experimentally, under our "standard conditions" acetone is the (neat) solvent making it impossible to change the concentration of acetone to probe its exact role in the observed nucleation and growth kinetics (i.e., and so long as one is in neat acetone). This led us to explore a cyclohexane-plus-acetone mixed solvent system, one that turned out to have nearly ideal experimental properties.[38,39] Specifically, we varied the acetone concentration from 0.5 to 2.7 M, while keeping the total volume of cyclohexane-plus-acetone constant at 2.5 mL. In each case, the supported-nanoparticle heterogeneous catalyst formation kinetics are sigmoidal and were again well-fit by the two-step mechanism. The extracted k_{2obs} and then also k_{1obs} versus [acetone] values are plotted in Figures 4 and 5, ○.

Qualitatively, both k_{2obs} and k_{1obs} show the predicted [acetone] dependence of eqs 6 and 5, respectively, over the range studied.[40] Conceptually, increasing the acetone concentration shifts the K_{Diss} equilibrium to the right, resulting in more, what turns out to be detectable [Ir(1,5-COD)Cl]$_2$, in solution (rather than Ir(1,5-COD)Cl(solvent)) under the mixed solvent conditions (see Figure S3) along with a concomitant increase in k_{2obs} and k_{1obs}.

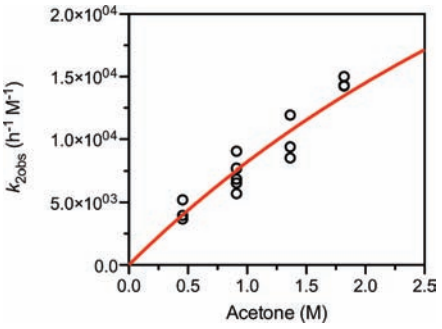

Figure 4. Dependence of the k_{2obs} rate constant on [acetone], ○. The red line is a weighted nonlinear least-squares fit to the slightly modified forms of eq 6 (a form of eq 6 that accounts for the formation of 1/2-[Ir(1,5-COD)Cl]$_2$ under the mixed-solvent conditions). The resultant K_{Diss}' and k_2''' values are 3(2) × 10^{-2} and 6(5) × 10^4 h^{-1} M^{-1}, respectively.

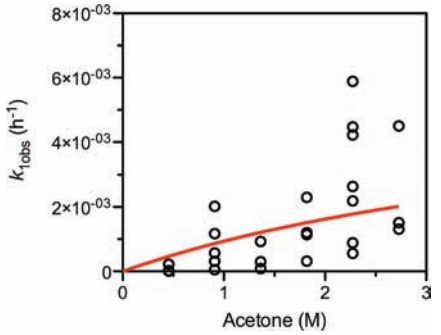

Figure 5. Dependence of the k_{1obs} rate constant on [acetone], ○. The red line is a weighted nonlinear least-squares fit to the slightly modified form of eq 5 (a form of eq 5 that accounts for the formation of 1/2-[Ir(1,5-COD)Cl]$_2$ under the mixed-solvent conditions). The value of K_{Diss}' was held constant at 0.03, and k_1'' was found to be 6(1) × 10^{-3} h^{-1}.

Significantly, we were able to confirm by UV−vis spectroscopy that the concentration of [Ir(1,5-COD)Cl]$_2$ in solution increases with increasing [acetone]. We were also able to obtain an independent verification of the K_{Diss} equilibrium in cyclohexane/acetone (vide infra), direct spectroscopic evidence consistent with [Ir(1,5-COD)Cl]$_2$ being a kinetically dominant intermediate en route to Ir(0)$_n$/γ-Al_2O_3 (as detailed further in the Supporting Information).

Quantitatively, we again first considered the k_{2obs} versus [γ-Al_2O_3]$_{sus}$ data (Figure 4, ○) due to the again anticipated large error in the k_{1obs} nucleation rate constants.[36] Because the [Ir(1,5-COD)Cl]$_2$ dimer forms in solution, slightly modified forms of eqs 5 and 6 needed to be, and were, derived (see eqs S36−S41 in the Supporting Information for the details of the kinetic treatment and resultant equations under the mixed, cyclohexane plus acetone solvent conditions). The relevant rate and equilibrium constants are now designated k_1'', k_2''', and K_{Diss}', due to their slight differences from the rate constants in Scheme 3, because of the presence of [Ir(1,5-COD)Cl]$_2$. Weighted nonlinear least-squares fitting of the k_{2obs} versus [acetone] data, using eq S41 (which has the same general form as eq 6), yielded values of k_2''' = 6(5) × 10^4 h^{-1} M^{-1} and K_{Diss}' = 3(2) × 10^{-2} (Figure 4, red line). We were again able to independently verify the K_{Diss}' equilibrium, this time by measuring the [Ir(1,5-COD)Cl]$_2$ in solution via UV−vis spectroscopy (Figure S3 of the Supporting Information). The spectroscopically determined value of K_{Diss}' was found to be 2.8(6) × 10^{-2}, identical within experimental error to the fit-determined K_{Diss}' value of 3(2) × 10^{-2}. The independent confirmation of the K_{Diss}' equilibrium is once again consistent with and fully supportive of the mechanism shown in Scheme 3. It also provides very strong support for the both the kinetic and UV−vis experiments and resultant data as well as the equations and methods used in their quantitative analysis.

Returning back to the k_{1obs} versus [acetone] data (Figure 5, ○), weighted nonlinear least-squares using eq S40 (which has the same general form as eq 5) again did not converge to unique k_1'' and K_{Diss}' values due to the expected and observed fluctuation in the k_{1obs} nucleation rate constants.[36] However, by constraining K_{Diss}' to its known value of 0.03, eq 6 could be used to account for at least the general shape of the k_{1obs} versus [acetone] data, Figure 5 (red line). An estimate of k_1'' = 6(1) × 10^{-3} h^{-1} resulted.

In summary of the [acetone] dependence kinetic and spectroscopic data, the k_{2obs} and k_{1obs} versus [acetone] data, as well as the increase in [Ir(1,5-COD)Cl]$_2$ in solution (monitored via UV−vis spectroscopy) with increasing acetone plus the independent confirmation of K_{Diss}', are all consistent with and supportive of the mechanism proposed in Scheme 3 (in bold).

Disproof of the "Heterogeneous" (i.e., All Solid-Oxide-Based) Nucleation (k_1) and Growth (k_2) and the "Homogeneous" (i.e., All Solution-Based) Growth Pathway (k_2'). While all of the kinetic, nanoparticle product[14] and spectroscopic or GLC data are consistent with and strongly supportive of the mechanism shown back in Scheme 3, as noted earlier we actually arrived at the mechanism in Scheme 3 by first (i) disproving the all solid-oxide-based (k_1 and k_2) nucleation and growth, and then (ii) disproving the all solution-based (k_2') growth pathways as detailed next.

The essence of those disproofs proceeded as follows. First, we considered the all solid-oxide-based, "heterogeneous" nucleation and growth pathway with the indicated rate constants, k_1 and k_2. The relevant rate equation (the full derivation of which is given in the Supporting Information) is identical to eq 4 except k_{1obs} and k_{2obs} are now given by eqs 7 and 8, respectively.

$$k_{1obs} = \frac{k_1[Al_2O_3]_{sus,t}}{[Al_2O_3]_{sus,t} + K_{Diss}[solvent]_t} \quad (7)$$

$$k_{2obs} = \frac{k_2[Al_2O_3]_{sus,t}}{[Al_2O_3]_{sus,t} + K_{Diss}[solvent]_t} \quad (8)$$

Inspection of eqs 7 and 8 reveals that k_{1obs} and k_{2obs} should increase with increasing [γ-Al_2O_3]$_{sus}$ if the all solid-oxide based, "heterogeneous" mechanism were correct. Of course and in fact, k_{2obs} and k_{1obs} decrease with increasing [γ-Al_2O_3]$_{sus}$ (Figures 2 and 3, respectively), effectively disproving the "heterogeneous" pathway. In addition, eqs 7 and 8 for the "heterogeneous" pathway predict that k_{1obs} and k_{2obs} will decrease with increasing [acetone], while Figures 4 and 5 reveal the opposite dependence: k_{1obs} and k_{2obs} increase with increasing [acetone]. In short, the [γ-Al_2O_3]$_{sus}$- and [acetone]-dependent kinetic data disprove the all solid-oxide-based, "heterogeneous" nucleation and growth mechanism.

Second, en route to the proposed mechanism in Scheme 3, we considered the case of an all solution-based, "homogeneous" nucleation and growth mechanism (k_1' and k_2'). The kinetic and

dx.doi.org/10.1021/ja110550h |J. Am. Chem. Soc. 2011, 133, 7744–7756

spectroscopic data (Supporting Information) presented so far are consistent with the solution-based nucleation pathway k_1'. However, the overall reaction stoichiometry (Ir(1,5-COD)Cl/γ-Al_2O_3 to Ir(0)$_n$/γ-Al_2O_3) is inconsistent with a solely, Ir(0)$_{n,soln}$ solution-based nanoparticle growth mechanism; the "weakly ligated/labile ligand" Ir(0)$_n$ nanoparticles are known to aggregate[14,20] and, therefore, typically give a broader size distribution then the ±14% that we experimentally observe.[14] It is thus necessary to introduce a fast, K_{Assoc} equilibrium, $[\gamma\text{-}Al_2O_3]_{sus}$ capture step to account for the observed, γ-Al_2O_3-supported Ir(0)$_{\sim 900}$ product. Such an assumption requires either (i) a size-dependent Ir(0)$_n$ K_{Assoc} equilibrium with $[\gamma\text{-}Al_2O_3]_{sus}$ or (ii) $k_2'K_{Assoc}$ to be fast relative to $k_2''K_{Assoc}'$. The relevant rate equation is identical to that of eq 4 (the full derivation of which is given in the Supporting Information), k_{1obs} is equivalent to eq 5, and k_{2obs} is now given by eq 9 for the putative "all homogeneous" mechanism.

$$k_{2obs} = \frac{k_2'K_{Diss}[solvent]_t}{K_{Assoc}[Al_2O_3]_{sus,t}^2 + K_{Diss}K_{Assoc}[Al_2O_3]_{sus,t}[solvent]_t} \quad (9)$$

Inspection of eq 9 reveals that k_{2obs} is proportional to an inverse-squared term in $[\gamma\text{-}Al_2O_3]_{sus}$, that is, to $1/[\gamma\text{-}Al_2O_3]_{sus}^2$. Attempts to fit the k_{2obs} versus $[\gamma\text{-}Al_2O_3]_{sus}$ data using eq 9 and by constraining K_{Diss} to its experimentally established value of 0.013 (and thus fitting for only two parameters) did not converge, arguing against and effectively disproving the solution-based nanoparticle growth pathway. In addition, simulations show that a $1/[\gamma\text{-}Al_2O_3]_{sus}^2$ dependence provides too-steep of a curve to fit the data, data that we know are tightly fit by eq 6 corresponding to the proposed mechanism, Figure 2.

In short, the $[\gamma\text{-}Al_2O_3]_{sus}$- and [acetone]-dependent k_{1obs} and k_{2obs} data (i) disprove the "heterogeneous" (i.e., all solid-oxide-based) nucleation and growth pathway (k_1 and k_2), while the k_{2obs} versus $[\gamma\text{-}Al_2O_3]_{sus}$ data (ii) disprove the "homogeneous" (i.e., all solution-based) Ir(0)$_n$ nanoparticle growth pathway (k_2').

Caveats: The Apparent Nature of the Rate and Equilibrium Constants, a Possible Role of Ir$_n$H$_m$ Species, and Comment Regarding Diffusional Processes. An important part of the present work is that it provides the first (semi)-quantitative, *but apparent*, values for the parameters k_1', k_1'', k_2'', k_2''' (K_{Diss} and K_{Diss}' were verified independently). That is, we wish to emphasize that all of these parameters should be regarded as apparent rate constants in a rigorous sense. Uncertainty arises in the precise, completely elementary/correct values for the rate constants determined herein as a result of primarily three sources: (i) the pseudo-order $[H_2]$ treatment[4] introduced from the cyclohexene reporter reaction kinetic monitoring method (see the Supporting Information for more details regarding the pseudo-order $[H_2]$ treatment); (ii) the treatment of γ-Al_2O_3 as a uniform, homogeneously suspended species with an effective "concentration"; and (iii) the inherent experimental[36] error in the nucleation and growth kinetic data. Hence, anyone using these first-of-their-kind rate "constants" needs to be aware of, and take into account, these uncertainties and the apparent nature of these parameters.

One additional caveat meriting mention is that where we write "Ir(0)$_n$/γ-Al_2O_3" (consistent with this being the demonstrated product[14]), it is possible that Ir$_n$H$_m$/γ-Al_2O_3 (i.e., hydride species) are what are actually the kinetically dominant form of Ir during the nucleation and early growth stages.[30,41] Noteworthy is that this same caveat, regarding the possible, but at present unsubstantiated, role of polymetallic hydrides in nanoparticle nucleation reactions, also exists in the extant mechanistic studies of nanoparticle formation in solution (see p 359 elsewhere[9]). Smaller, polymetallic metal hydrides as one possible key intermediate in nanoparticle nucleation and growth is a topic meriting careful experimental study, in our opinion, a topic we are currently addressing.

The careful reader will also have noted that we have not addressed any issues associated with the more complex nature of the γ-Al_2O_3 support, including its ca. ∼100 μm pellet and ca. 5.8 nm pore size (manufacturers specifications), in relation to diffusion. We can, however, rule out diffusion-limited processes because the kinetic data can be fit to the chemical-reaction-rate limited, two-step mechanism. Our kinetic data require that any diffusional processes be fast relative to the A → B and A + B → 2B chemical-reaction rate-determining steps that we measure. An additional point relevant to diffusion, pointed out by an insightful referee (that we thank), is that 2.9 nm Ir(0)$_{\sim 900}$ nanoparticles likely will not readily diffuse through the 5.8 nm γ-Al_2O_3 pores, yet the final Ir(0)$_{\sim 900}$ nanoparticles are well dispersed throughout the γ-Al_2O_3 (see the TEM images in Scheme 1). We agree and note that these observations support the proposed mechanism in Scheme 3 in which smaller, Ir(0)$_n$ nanoparticles are captured by the γ-Al_2O_3.[42,43] Those particles then grow via the chemical-reaction limited autocatalytic surface growth step (i.e., A + B → 2B) from Ir(1,5-COD)Cl(solvent) in solution. In other words, all of our experimental evidence indicates that the overall supported-nanoparticle heterogeneous catalyst formation reaction (in contact with solution) is chemical-reaction-rate limited and not diffusion limited.

Desirable, future studies include, then: (i) a precise determination of the concentration of "Ir(1,5-COD)Cl" binding sites on the γ-Al_2O_3; (ii) direct observation and kinetic measurements of the Ir(1,5-COD)Cl/γ-Al_2O_3 to Ir(0)$_n$/γ-Al_2O_3 supported-nanoparticle heterogeneous catalyst formation under in situ, or better under operating (i.e., "operando"), conditions; (iii) direct evidence for or against possible "Ir$_n$H$_m$" intermediates; and (iv) independent direct measurement and verification or refinement of the key, apparent parameters k_1', k_1'', k_2'', and k_2'''. Despite these needed additional studies, the present study is still the first of its kind, and as such provides both the specific parameters to be verified or updated as well as the general mechanistic scheme, Scheme 3, around which one can now design additional measurements.

A Comparison of Solid-Oxide-Supported Ir(1,5-COD)Cl/γ-Al_2O_3 to Ir(0)$_{\sim 900}$/γ-Al_2O_3 Nanoparticle Formation to Polyoxoanion-Supported and Stabilized Ir(1,5-COD)·$P_2W_{15}Nb_3O_{62}^{8-}$ to Ir(0)$_{\sim 300}$·$(P_2W_{15}Nb_3O_{62}^{8-})_n^{-8n}$ Nanoparticle Formation in Solution. The Ir(1,5-COD)Cl/γ-Al_2O_3 to Ir(0)$_{\sim 900}$/γ-Al_2O_3 nanoparticle formation system allows an interesting, first-of-its-kind, comparison to the kinetically and mechanistically well-studied $[Ir(1,5\text{-}COD)\cdot P_2W_{15}Nb_3O_{62}]^{8-}$ to Ir(0)$_{\sim 300}$·$(P_2W_{15}Nb_3O_{62}^{8-})_n^{-8n}$ nanoparticle formation system in solution,[4,45,34] Scheme 4, top.

Comparison of the Ir(1,5-COD)Cl/γ-Al_2O_3 to Ir(0)$_{\sim 900}$/γ-Al_2O_3 system herein, Scheme 1, to the polyoxoanion supported and stabilized system in Scheme 4, reveals two striking similarities between the supported- and solution-based systems, specifically the involvement in both systems of (i) a dissociated, solution-based Ir(1,5-COD)$^+$ moiety, and (ii) a solution-based nucleation mechanism under H_2 to Ir(0)$_n$. In the case of the

Scheme 4. The Kinetically and Mechanistically Well-Studied $Ir(1,5\text{-}COD)\cdot P_2W_{15}Nb_3O_{62}]^{8-}$ to $Ir(0)_{\sim 300}\cdot(P_2W_{15}Nb_3O_{62}{}^{8-})_n{}^{-8n}$, Soluble, Nanoparticle Formation System (Top) and Its $Ir(1,5\text{-}COD)^+$-Based, Dissociative Equilibrium En Route to $Ir(0)_{\sim 300}\cdot(P_2W_{15}Nb_3O_{62}{}^{8-})_n{}^{-8n}$ Nanoparticle Formation

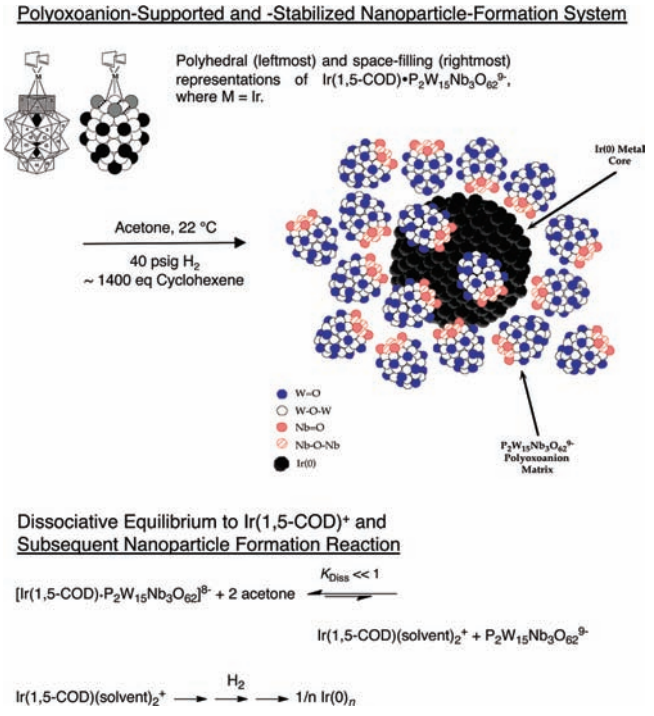

polyoxoanion-supported system, evidence for a dissociative equilibrium to $Ir(1,5\text{-}COD)(solvent)_2{}^+$ was first obtained in 1994 starting from the $[Ir(1,5\text{-}COD)\cdot P_2W_{15}Nb_3O_{62}]^{8-}$ precatalyst and en route to soluble, polyoxoanion stabilized ("supported") $Ir(0)_{\sim 300}\cdot(P_2W_{15}Nb_3O_{62}{}^{8-})_n{}^{-8n}$, Scheme 4, bottom.[34b] Key evidence at the time for a $[Ir(1,5\text{-}COD)\cdot P_2W_{15}Nb_3O_{62}]^{8-}$ to $Ir(1,5\text{-}COD)(solvent)_2{}^+$ dissociative equilibrium included: (i) a solvent dependency,[33,34b] similar to that in Table 1 (i.e., facile kinetics were observed in the coordinating solvent acetone, but were much slower in the less coordinating solvent CH_2Cl_2), (ii) demonstration that small amounts of added $P_2W_{15}Nb_3O_{62}{}^{9-}$ dramatically inhibit the nanoparticle formation kinetics,[4,44] and (iii) the demonstration that trace amounts of $Ir(1,5\text{-}COD)(solvent)_2{}^+$ significantly accelerated the nanoparticle formation kinetics (especially reducing the nucleation time),[4,44] direct kinetic evidence for the involvement of $Ir(1,5\text{-}COD)(solvent)_2{}^+$ in the nucleation and growth processes. Overall, the solvent, $P_2W_{15}Nb_3O_{62}{}^{9-}$, and $Ir(1,5\text{-}COD)(solvent)_2{}^+$ dependent kinetic data are strongly supportive of the K_{Diss} equilibrium shown in Scheme 4, a key step in the mechanism that parallels the kinetically dominant, Ir(1,5-COD)Cl(solvent), and K_{Diss} pathway back in Scheme 3.

In summary, this first comparison between solid- versus polyoxoanion-soluble oxide-supported nanoparticle formation systems (i) reveals striking similarities in their mechanisms, specifically that both involve (a) dissociated, solution-based $Ir(1,5\text{-}COD)^+$ (or Ir(1,5-COD)Cl) moieties, and (b) solution nucleation under H_2 to $Ir(0)_n$; (ii) reveal the value of having the soluble $Ir(0)_{\sim 300}\cdot(P_2W_{15}Nb_3O_{62}{}^{8-})_n{}^{-8n}$ nanoparticle formation system and its kinetics already in hand for such qualitative comparisons, and (iii) satisfies criterion number seven of our previous definition[14,32] of the key attributes of a prototype, solid-oxide supported nanoparticle formation system in contact with solution, namely that such a comparison be possible and made. The comparison of the soluble, polyoxoanion-based oxide and solid-oxide systems also (iv) provides the best test to date of the long-standing hypothesis that custom-made polyoxoanions can serve as "soluble metal-oxide analogues",[4,34,45] and (v) provides the strongest evidence to date in support of the "soluble metal-oxide analogues" hypothesis.

CONCLUSIONS

Herein, we have continued to pursue the global hypothesis that quantitative kinetic and mechanistic studies of supported-nanoparticle heterogeneous catalyst formation, in contact with solution, will allow exploration of an important, but to-date little investigated, subarea of heterogeneous catalyst synthesis—specifically, the transformation of solid-supported organometallics into supported-nanoparticle catalysts while in contact with solution. The solvent variation-, γ-Al_2O_3-, and acetone-dependent kinetic data (as well as GLC and UV−vis spectroscopic data) are all consistent with and strongly supportive of nucleation occurring from the dissociated Ir(1,5-COD)Cl(solvent) complex in solution, fast $Ir(0)_n$ nanoparticle capture by γ-Al_2O_3, and subsequent solid-oxide-supported nanoparticle growth between $Ir(0)_n/\gamma$-Al_2O_3 and Ir(1,5-COD)Cl(solvent). The kinetic data disprove the $Ir(1,5\text{-}COD)Cl/\gamma\text{-}Al_2O_3$ "heterogeneous" (i.e., all solid-oxide-based) nucleation and growth mechanism (i.e., the k_1 and k_2 pathways back in Scheme 3) as well any "homogeneous" (i.e., all solution-based) nanoparticle growth pathway involving Ir(1,5-COD)Cl(solvent) (i.e., such as k_2', Scheme 3).

We expect the finding of solution-based nucleation to prove more general for (i) other coordinatively saturated (e.g., d^8 square planar) supported-organometallic species, that is, supported complexes that do not have facile reduction mechanisms to $M(0)_n$ under H_2 (i.e., and while still on the support), and for (ii) other high-valent supported organometallics and metal salts (e.g., Ir(III), Rh(III), Au(III), and so on) that may not also have facile H_2 activation[45] mechanisms to $M(0)_n$ when supported. The kinetic studies herein have also allowed the first experimental estimations of the associated k_1', k_1'', k_2'', k_2''' apparent rate constants and the K_{Diss} and K_{Diss}' equilibrium constants defined in Scheme 3. Comparative studies of the $Ir(1,5\text{-}COD)Cl/\gamma\text{-}Al_2O_3$ to $Ir(0)_{\sim 900}/\gamma\text{-}Al_2O_3$ nanoparticle formation system in contact with solution to the kinetically and mechanistically well-studied $Ir(1,5\text{-}COD)\cdot P_2W_{15}Nb_3O_{62}{}^{8-}$ to $Ir(0)_{\sim 300}\cdot(P_2W_{15}Nb_3O_{62}{}^{8-})_n{}^{-8n}$ solution nanoparticle formation system, revealed closely similar $Ir(1,5\text{-}COD)^+$ (and Ir(1,5-COD)Cl) dissociation, solution-based nucleation mechanisms.[4,34b] That comparison also provided the first compelling evidence that suitable, custom-made polyoxoanions can function as soluble models/analogues of solid-oxide-supported heterogeneous catalysts ("soluble heterogeneous catalyst analogues").[46]

Looking forward, it seems reasonable to expect that supported-nanoparticle heterogeneous catalyst formation in contact with solution may yield a more direct avenue for transferring both the synthetic and the mechanistic insights, which have resulted from the modern revolution in nanoparticle science in solution, to supported-nanoparticle heterogeneous

dx.doi.org/10.1021/ja110550h |J. Am. Chem. Soc. 2011, 133, 7744–7756

catalysts and their subsequent catalysis. Our own additional studies in this direction are continuing and will be reported in due course.

EXPERIMENTAL SECTION

Materials. All solvents and compounds used were stored in the drybox prior to use. Used as received were the following (all of which came sealed under N_2): acetone (Burdick & Jackson, water content <0.5%), anhydrous cyclohexane (Aldrich, 99.5%), anhydrous CH_2Cl_2 (Aldrich, ≥99.8%), anhydrous propylene carbonate (Aldrich, 99.7%), and $[Ir(1,5\text{-COD})Cl]_2$ (STREM, 99%). Cyclohexene (Aldrich, 99%) was freshly distilled over Na metal and under argon or purified via a MicroSolv solvent purification system (Innovative Technology) using an activated γ-Al_2O_3 column under N_2. Ethyl acetate (Aldrich, ≥99.8%, <0.05% H_2O) was degassed prior to use in the drybox. Acidic activated γ-Al_2O_3 (Aldrich), with a surface area of 155 m^2/g, was dried at 160 °C in air for 24 h (the average relative humidity in Fort Collins, CO ranges from ∼38% to ∼72% over the course of the year[47−49]). H_2 gas purchased from Airgas (>99.5% purity) was passed through O_2- and H_2O-scavenging traps (Trigon Technologies) before use.

Analytical Instrumentation and Procedures. Unless otherwise reported, all reaction solutions were prepared under O_2- and moisture-free conditions in a Vacuum Atmospheres N_2-filled drybox. The O_2 level (always ≤5 ppm; typically ≤1 ppm) was continuously monitored by a Vacuum Atmospheres O_2 sensor. GLC was performed using a Hewlett-Packard 5890 Series II chromatograph, along with a flame-ionization detector and equipped with a Supelco SPB-1 (Aldrich, 30 m × 0.25 mm × 0.25 μm) fused silica column. The GLC parameters were as follows: initial oven temperature, 50 °C; initial time, 3.0 min; rate, 10 °C/min; final temperature, 160 °C; injector temperature, 180 °C; detector temperature, 200 °C; and injection volume, 2 μL. UV−vis spectroscopy experiments were run on a Hewlett-Packard 8452A diode array spectrophotometer, and the data were analyzed via Hewlett-Packard's UV−vis ChemStation software.

Hydrogenation Apparatus and Data Handling. Hydrogenation experiments for monitoring the H_2 reduction of Ir(1,5-COD)Cl/γ-Al_2O_3 to $Ir(0)_n$/γ-Al_2O_3 were carried out in a previously described apparatus,[4−8] which continuously monitors the H_2 pressure loss. Briefly, the apparatus consists of a Fisher-Porter (FP) bottle modified with Swagelok TFE-sealed Quick-Connects to both a H_2 line and an Omega PX621 pressure transducer. The pressure transducer is interfaced to a PC through an Omega D1131 5 V A/D converter with a RS-232 connection. Reactions were run at a constant temperature by immersing the FP bottle in a 500 mL jacketed reaction flask containing dimethyl silicon fluid (Thomas Scientific), the temperature of which was regulated by a thermostatted recirculating water bath (VWR). Pressure uptake data were collected using LabView 7.1. The hydrogen uptake curves were then converted to cyclohexene (M) curves using the previously established 1:1 H_2/cyclohexene stoichiometry.[4,34] The data were also corrected for the acetone solvent vapor pressure using the previously established protocol.[45] Specifically, one can either measure the acetone vapor pressure independently and subtract that curve (point-by-point) from the raw H_2 uptake data during the cyclohexene reporter reaction, or one can simply back extrapolate the experimental vapor pressure rise (seen in the induction period of the reaction). Both methods yield the same k_1 and k_2 rate constants within ±15%.[45] The resultant cyclohexene loss kinetic curves were fit to the two-step analytic equation[4] for nucleation and autocatalytic surface growth of nanoparticle formation, A → B, rate constant k_1, plus A + B → 2B, rate constant k_2 (see Scheme 2), using nonlinear least-squares fitting in Origin 7.0.

The k_{1obs} and k_{2obs} versus $[\gamma\text{-}Al_2O_3]_{sus}$ and [acetone] curves were fit using weighted nonlinear least-squares analysis in GraphPad Prism 5.0. Relative weighting (i.e., $1/Y^2$) was used as the average absolute distance, between the curve and the data points, is larger when Y is larger. Use of $1/Y^2$ weighted nonlinear least-squares analysis minimizes the sum-of-squares of eq 10.[50,51] For the $[\gamma\text{-}Al_2O_3]_{sus}$-dependent k_{1obs} and k_{2obs} curve-fitting, [acetone] was taken to be constant at a value of 11.37 M. For the [acetone]-dependent fitting, $[\gamma\text{-}Al_2O_3]_{sus}$ was taken to be constant at a value of 0.163 M.

$$\sum \frac{1}{Y^2}\left(Y_{Data} - Y_{Curve}\right)^2 \qquad (10)$$

Precatalyst Preparation. All of the precatalysts were prepared in a drybox using preselected $[Ir(1,5\text{-COD})Cl]_2$/γ-Al_2O_3 weight-to-weight ratios. For example, a 2.0% weight-to-weight Ir(1,5-COD)Cl/γ-Al_2O_3 sample was prepared by adding 1.0 g of acidic γ-Al_2O_3 to 20 mg of $[Ir(1,5\text{-COD})Cl]_2$ corresponding to a 2.0 wt % sample (i.e., wt % = [wt $[Ir(1,5\text{-COD})Cl]_2$/(wt $[Ir(1,5\text{-COD})Cl]_2$+ wt γ-Al_2O_3)] × 100, as this is what we experimentally measure out and hence know), by the following procedure. The appropriate amount of $[Ir(1,5\text{-COD})Cl]_2$ was weighed out in a 20 mL scintillation vial. A new 5/8 in. × 5/16 in. Teflon-coated octagon-shaped stir bar was added to the vial, and the solid was dissolved in 15 mL of ethyl acetate. Subsequently, the appropriate amount of solid oxide (e.g., 1.0 g of acidic γ-Al_2O_3 for the 2.0 wt % Ir catalyst) was added by pouring the metal oxide into the vial (i.e., this order of addition is deliberate; see p 9712 of our prior publication for why this is important[14]), and the solution was stirred for 24 h to equilibrate the $[Ir(1,5\text{-COD})Cl]_2$ with the solid oxide and the solution. After a 24 h equilibration period, the slurry was taken to dryness in the drybox by placing the sample under vacuum for 8 h at room temperature. The resulting supported precatalysts were then stored in the drybox.

Solvent-Dependent Nucleation and Growth Kinetics: A Standard Conditions Reaction. In a drybox, 0.05 g of the Ir(1,5-COD)Cl/γ-Al_2O_3 catalyst precursor was weighed out into a 2-dram vial and transferred to a culture tube (22 × 175 mm) with a new 5/8 in. × 5/16 in. Teflon-coated octagon-shaped stir bar. To ensure a quantitative transfer, 2.5 mL of acetone and 0.5 mL of cyclohexene were added to the 2-dram vial, and transferred via a disposable polyethylene pipet into the same borosilicate culture tube containing the Ir(1,5-COD)Cl/γ-Al_2O_3 precatalyst. The culture tube was then sealed in the FP bottle, removed from the drybox, and attached to the H_2 line. The sealed, H_2-line attached FP bottle was placed into a temperature regulated water bath set at 22.0 ± 0.1 °C. A standard conditions purge cycle was used to initiate the reaction where a series of H_2-flushing cycles in which the FP bottle is purged with H_2 every 15 s until 3.5 min have passed (a total of 14 purges). The stir plate was started and set at 600 rpm to allow the H_2 gas-to-solution equilibrium, and the H_2 pressure was then set to 40 psig with the data recording started at 4 min after the purge cycle began (which defined t = 0 for the kinetics).

Variation of the $[\gamma\text{-}Al_2O_3]_{sus}$. As described in the Standard Conditions Reaction section, 0.05 g of the Ir(1,5-COD)Cl/γ-Al_2O_3 catalyst precursor was weighed out into a 2-dram vial and transferred to a culture tube. To ensure quantitative transfer, 2.5 mL of the appropriate solvent was placed into the 2-dram vial and transferred via a polyethylene disposable pipet into the same culture tube. Next, the preselected amount of 160 °C dried γ-Al_2O_3 was weighed out into a separate 2-dram vial and transferred into the same culture tube. The reaction slurry (i.e., the 0.05 g of precatalyst, the 2.5 mL of acetone, and the additional γ-Al_2O_3) was sealed in the borosilicate culture tube and stirred in the drybox for 8 h. Control reactions demonstrated that equilibration periods >8 h, for both the low (0.25 M) and the high (0.98 M) $[\gamma\text{-}Al_2O_3]_{sus}$, did not affect the resultant nucleation and growth kinetics. After the 8 h stirring period, 0.5 mL of cyclohexene was added to the slurry. The borosilicate culture tube was then placed in

a FP bottle, and a Standard Conditions Reaction was initiated as described above.

Variation of the Acetone Concentration: Cyclohexane/Acetone Mixed Solvent Conditions. In a drybox, 50 mg of the 2.0 wt % Ir(1,5-COD)Cl/γ-Al_2O_3 prototype precatalyst was weighed out into a 20 mL scintillation vial, and a new 5/8 in. × 5/16 in. Teflon-coated octagon-shaped stir bar was added. Subsequently, 2.5 mL of the prechosen cyclohexane/acetone mixture (vide supra) was added, and the slurry was stirred for 24 h in the drybox. After the 24 h stirring equilibration period, 0.5 mL of cyclohexene was added to the slurry and was transferred via a disposable polyethylene pipet into a new borosilicate culture tube (22 × 175 mm) with a new 5/8 in. × 5/16 in. Teflon-coated octagon-shaped stir bar, and then a Standard Conditions Reaction was initiated as described above. At $[Ir(1,5\text{-}COD)Cl]_2$ concentrations above ~0.2 mM, stirring speeds of 1000 rpm were necessary to maximize H_2 gas-to-solution mass transfer.[40]

Independent Verification of the Loss of Ir(1,5-COD)Cl-(Solvent) via UV−Vis Spectroscopy and K_{Diss} via GLC and the Formation of $[Ir(1,5\text{-}COD)Cl]_2$ and K_{Diss}' via UV−Vis Spectroscopy. Control reactions done to probe if Ir(1,5-COD)Cl-(solvent) decreases with increasing $[\gamma\text{-}Al_2O_3]_{sus}$ were all done under O_2-free conditions (i.e., in the drybox). To start, 0.05 g of the 2.0 wt % Ir(1,5-COD)Cl/γ-Al_2O_3 precatalyst was placed in a 20 mL scintillation vial along with 2.5 mL of acetone. Subsequently, the appropriate amount of additional γ-Al_2O_3 (0.25−0.65 M) was added, and the slurry was stirred for 8 h. The slurry was then filtered through a 0.2 μm nylon filter (NALGENE) and into an O_2 free UV−vis cell, sealed, and then brought out of the drybox; the visible spectrum was then recorded. K_{Diss} was independently verified in nearly an identical manner, except 0.5 mL of cyclohexene along with 2 μL of decane (as an internal standard) were added to the filtered solution of Ir(1,5-COD)Cl(solvent), and a standard conditions hydrogenation was run (employing the same purge cycle, etc., as described above). Upon completion of the hydrogenation of cyclohexene, GLC was used to determine the quantity of cyclooctane in solution.

Control reactions, all done under O_2 free conditions, to determine if $[Ir(1,5\text{-}COD)Cl]_2$ increased with increasing [acetone] were run from 0.14 to 2.7 M [acetone]. To start, 0.05 g of the 2.0 wt % Ir(1,5-COD)Cl/γ-Al_2O_3 precatalyst was placed in a 20 mL scintillation vial along with 2.5 mL of the total mixed solvent (i.e., cyclohexane + acetone = 2.5 mL). The slurry was then filtered through a 0.2 μm nylon filter into an O_2 free UV−vis cell.

■ ASSOCIATED CONTENT

Ⓢ Supporting Information. Solvent-dependent supported-nanoparticle heterogeneous catalyst formation kinetics and their fits to the two-step mechanism; kinetic derivation of the proposed mechanism (k_1' and k_2''), Scheme 3 (bold); kinetic derivation for the "heterogeneous" (i.e., all solid-oxide-based) nucleation (k_1) and growth (k_2) mechanism; kinetic derivation for the "homogeneous" (i.e., all solution-based) nucleation (k_1') and growth (k_2') mechanism; mechanistic and curve fitting treatment of k_{1obs} and k_{2obs} versus [acetone]; comparison of the loss of Ir(1,5-COD)Cl(solvent) and the decrease in k_{1obs} and k_{2obs} with increasing $[\gamma\text{-}Al_2O_3]_{sus}$; comparison of the increase in $[Ir(1,5\text{-}COD)Cl]_2$ and the increase in k_{1obs} and k_{2obs} with increasing [acetone]; further consideration and use of the direct GLC and spectroscopic data to independently calculate K_{Diss} and K_{Diss}'; and discussion of direct spectroscopic monitoring of the Ir(1,5-COD)Cl/γ-Al_2O_3 to $Ir(0)_n$/γ-Al_2O_3 supported-nanoparticle formation reaction. This material is available free of charge via the Internet at http://pubs.acs.org.

■ AUTHOR INFORMATION

Corresponding Author
rfinke@lamar.colostate.edu

■ ACKNOWLEDGMENT

We gratefully acknowledge support from the Chemical Sciences, Geosciences, and Biosciences Division, Office of Basic Energy Sciences, Office of Science, U.S. Department of Energy, Grant SE-FG02-03ER15453.

■ REFERENCES

(1) (a) Gates, B. C. *Catalytic Chemistry*; John Wiley & Sons: New York, 1992. (b) Bartholomew, C. H.; Farrauto, R. J. *Fundamentals of Industrial Catalytic Processes*, 2nd ed.; John Wiley & Sons: Hoboken, 2006.

(2) Schlögl, R.; Abd, H.; S., B. *Angew. Chem., Int. Ed.* **2004**, *43*, 1628.

(3) Some recent reviews on the synthesis of transition metal nanoparticles include (please see also the extensive references therein for additional, earlier reviews of nanoparticle chemistry): (a) Aiken, J. D., III; Finke, R. G. *J. Mol. Catal. A: Chem.* **1999**, *145*, 1. (b) Crooks, R. M.; Zhao, M.; Sun, L.; Chechik, V.; Yeung, L. K. *Acc. Chem. Res.* **2001**, *34*, 181. (c) Bönnemann, H.; Richards, R. M. *Eur. J. Inorg. Chem.* **2001**, 2455. (d) Roucoux, A.; Schulz, J.; Patin, H. *Chem. Rev.* **2002**, *102*, 3757. (e) Cushing, B. L.; Kolesnichenko, V. L.; O'Connor, C. J. *Chem. Rev.* **2004**, *104*, 3893. (f) Astruc, D.; Lu, F.; Aranzaes, J. R. *Angew. Chem., Int. Ed.* **2005**, *44*, 7852. (g) Wilcoxon, J. P.; Abrams, B. L. *Chem. Soc. Rev.* **2006**, *35*, 1162. (h) Ott, L. S.; Finke, R. G. *Coord. Chem. Rev.* **2007**, *251*, 1075. (i) Semagina, N.; Kiwi-Minsker, L. *Catal. Rev.-Sci. Eng.* **2009**, *51*, 147.

(4) Watzky, M. A.; Finke, R. G. *J. Am. Chem. Soc.* **1997**, *119*, 10382. See also the table in the Supporting Information therein of the 19 prior key papers, which constituted the nanoparticle formation mechanism literature prior to 1997.

(5) Hornstein, B. J.; Finke, R. G. *Chem. Mater.* **2004**, *16*, 139; See also: *Chem. Mater.* **2004**, *16*, 3972.

(6) Besson, C.; Finney, E. E.; Finke, R. G. *J. Am. Chem. Soc.* **2005**, *127*, 8179.

(7) Besson, C.; Finney, E. E.; Finke, R. G. *Chem. Mater.* **2005**, *17* 4925.

(8) Finney, E. E.; Finke, R. G. *Chem. Mater.* **2008**, *20*, 1956.

(9) A recent review of the kinetic and mechanistic studies of transition-metal nanoparticle nucleation and growth, with an emphasis on the nucleation process, has appeared: Finney, E. E.; Finke, R. G. *J. Colloid Interface Sci.* **2008**, *317*, 351.

(10) Some additional recent references, to the growing mechanistic insights into the synthesis of transition-metal nanoparticles resulting from the modern revolution in nanoparticle science, include: (a) Zheng, H.; Smith, R. K.; Jun, Y.-W.; Kisielowski, C.; Dahmen, U.; Alivisatos, A. P. *Science* **2009**, *324*, 1309. (b) Murray, C. B. *Science* **2009**, *324*, 1276. (c) Harada, M.; Inada, Y. *Langmuir* **2009**, *25*, 6049. (d) Polte, J.; Ahner, T. T.; Delissen, F.; Sokolov, S.; Emmerling, F.; Thunemann, A. F.; Kraehnert, R. *J. Am. Chem. Soc.* **2010**, *132*, 1296. (e) Polte, J.; Erler, R.; Thunemann, A. F.; Sokolov, S.; Ahner, T. T.; Rademann, K.; Emmerling, F.; Kraehnert, R. *ACS Nano* **2010**, *4*, 1076. (f) Yao, T.; Sun, Z.; Li, Y.; Pan, Z.; Wei, H.; Xie, Y.; Nomura, M.; Niwa, Y.; Yan, W.; Wu, Z.; Jiang, Y.; Liu, Q.; Wei, S. *J. Am. Chem. Soc.* **2010**, *130*, 7696.

(11) Discrete, atomically precise nanoparticles (or nanoclusters) are known in the literature; for example, see: (a) Mednikov, E. G.; Jewell, M. C.; Dahl, L. F. *J. Am. Chem. Soc.* **2007**, *129*, 11619–11630. Also see the extensive references therein for similar nanosized clusters. (b) Jadzinsky, P. D.; Calero, G.; Ackerson, C. J.; Bushnell, D. A.; Kornberg, R. D. *Science* **2007**, *318*, 430. (c) Shichibu, Y.; Negishi, Y.; Watanabe, T.; Chaki, N. K.; Kawaguchi, H.; Tsukuda, T. *J. Phys. Chem. C* **2007**, *111*, 7845. (d) Zhu, M.; Aikens, C. M.; Hollander, F. J.; Schatz, G. C.; Jin,

R. *J. Am. Chem. Soc.* **2008**, *130*, 5883. (e) Heaven, M. W.; Dass, A.; White, P. S.; Holt, K. M.; Murray, R. W. *J. Am. Chem. Soc.* **2008**, *130*, 3754.

(12) Corain, B., Schmid, G., Toshima, N., Eds. *Metal Nanoparticles in Catalysis and Materials Science: The Issue of Size Control*; Elsevier: Amsterdam, 2008.

(13) (a) Ahmadi, T. S.; Wang, Z. L.; Green, T. C.; Henglein, A.; El-Sayed, M. A. *Science* **1996**, *272*, 1924. (b) Burda, C.; Chen, X.; Narayanan, R.; El-Sayed, M. A. *Chem. Rev.* **2005**, *105*, 1025. (c) Tao, A. R.; Habas, S.; Yang, P. *Small* **2008**, *4*, 310. (d) Xia, Y.; Xiong, Y.; Lim, B.; Skrabalak, S. E. *Angew. Chem., Int. Ed.* **2009**, *48*, 60.

(14) Mondloch, J. E.; Wang, Q.; Frenkel, A. I.; Finke, R. G. *J. Am. Chem. Soc.* **2010**, *132*, 9701.

(15) Examples where preformed nanoparticles are deposited onto supports can be found in the following references: (a) Kónya, Z.; Puntes, V. F.; Kiricsi, I.; Zhu, J.; Ager, J. W., III; Ko, M. K.; Frei, H.; Alivisatos, P.; Somorjai, G. A. *Chem. Mater.* **2003**, *15*, 1242. (b) Zheng, N.; Stucky, G. D. *J. Am. Chem. Soc.* **2006**, *128*, 14278. (c) Lee, I.; Morales, R.; Albiter, M. A.; Zaera, F. *Proc. Natl. Acad. Sci. U.S.A.* **2008**, *105*, 15241. (d) Huang, X.; Guo, C.; Zuo, J.; Zheng, N.; Stucky, G. D. *Small* **2009**, *5*, 361. (e) Boualleg, M.; Basset, J.-M.; Candy, J.-P.; Delichere, P.; Pelzer, K.; Veyre, L.; Thieuleux, C. *Chem. Mater.* **2009**, *21*, 775. (f) Zhu, Y.; Qian, H.; Drake, B. A.; Jin, R. *Angew. Chem., Int. Ed.* **2010**, *49*, 1.

(16) Examples from Somorjai and co-workers are available where they have made extensive, expert efforts to remove stabilizing ligand overlayers from both $Pt(0)_n$ and $Rh(0)_n$ nanoparticles with varying, albeit never complete, degrees of success: (a) Rioux, R. M.; Song, H.; Hoefelmeyer, J. D.; Yang, P.; Somorjai, G. A. *J. Phys. Chem. B* **2005**, *109*, 2192. (b) Song, H.; Rioux, R. M.; Hoefelmeyer, J. D.; Komor, R.; Niesz, K.; Grass, M.; Yang, P.; Somorjai, G. A. *J. Am. Chem. Soc.* **2006**, *128*, 3027. (c) Rioux, R. M.; Hsu, B. B.; Grass, M. E.; Song, H.; Somorjai, G. A. *Catal. Lett.* **2008**, *126*, 10. (d) Borodko, Y.; Jones, L.; Lee, H.; Frei, H.; Somorjai, G. A. *Langmuir* **2009**, *25*, 6665. (e) Park, J. Y.; Aliaga, C.; Russell Renzas, J.; Lee, H.; Somorjai, G. A. *Catal. Lett.* **2009**, *129*, 1. (f) Aliaga, C.; Park, J. Y.; Yamada, Y.; Sook Lee, H.; Tsung, C.-H.; Yang, P.; Somorjai, G. A. *J. Phys. Chem. C* **2009**, *113*, 6150. (g) Grass, M. E.; Joo, S. H.; Zhang, Y.; Somorjai, G. A. *J. Phys. Chem. C* **2009**, *113*, 8616. (h) Borodko, Y. G.; Lee, H. Y.; Joo, S. H.; Zhang, Y.; Somorjai, G. A. *J. Phys. Chem. C* **2010**, *114*, 1117. (i) Kuhn, J. N.; Tsung, C.-H.; Huang, W.; Somorjai, G. A. *J. Catal.* **2009**, 209. There are also extensive examples attempting to remove dendrimer stabilizers, from dendrimer-stabilzed and supported nanoparticles; see, for example:(j) Lang, H.; May, A.; L., I. B.; Chandler, B. D. *J. Am. Chem. Soc.* **2003**, *125*, 14832. (k) Liu, D.; Gao, J.; Murphy, C. J.; Williams, C. T. *J. Phys. Chem. B* **2004**, *108*, 12911. (l) Singh, A.; Chandler, B. D. *Langmuir* **2005**, *21*, 10776. (m) Deutsch, D. S.; Siani, A.; Fanson, P. T.; Hirata, H.; Matsumoto, S.; Williams, C. T.; Amiridis, M. D. *J. Phys. Chem. C* **2007**, *111*, 4246. (n) Albiter, M. A.; Zaera, F. *Langmuir* **2010**, *26*, 16204.

(17) Mondloch, J. E.; Yan, X.; Finke, R. G. *J. Am. Chem. Soc.* **2009**, *131*, 6389.

(18) Additional examples of supported-nanoparticle heterogeneous catalyst preparation in contact with solution include: (a) De Jong, K. P.; Geus, J. W. *Appl. Catal., A* **1982**, *4*, 41. (b) Bond, G. C.; Rawle, A. F. *J. Mol. Catal. A: Chem.* **1996**, *109*, 261. (c) Sales, E. A.; Benhamida, B.; Caizergues, V.; Lagier, J.-P.; Fievet, F.; Bozon-Verduraz, F. *Appl. Catal., A* **1998**, *172*, 273. (d) Guari, Y.; Thieuleux, C.; Mehdi, A.; Reyé, C.; Corriu, R. J. P.; Gomez-Gallardo, S.; Philippot, K.; Chaudret, B.; Dutartre, R. *Chem. Commun.* **2001**, 1374. (e) Guari, Y.; Thieuleux, C.; Mehdi, A.; Reyé, C.; Corriu, R. J. P.; Gomez-Gallardo, S.; Philippot, K.; Chaudret, B. *Chem. Mater.* **2003**, *15*, 2017. (f) Marconi, G.; Pertici, P.; Evangelisti, C.; Caporusso, A. M.; Vitulli, G.; Capannelli, G.; Hoang, M.; Turney, T. W. *J. Organomet. Chem.* **2004**, *689*, 639. (g) Hulea, V.; Brunel, D.; Galarneau, A.; Philippot, K.; Chaudret, B.; Kooyman, P. J.; Fajula, F. *Microporous Mesoporous Mater.* **2005**, *79*, 185. (h) Jiang, Y.; Gao, Q. *J. Am. Chem. Soc.* **2006**, *128*, 716. (i) Zhong, L.-S.; Hu, J.-S.; Cui, Z.-M.; Wan, L.-J.; Song, W.-G. *Chem. Mater.* **2007**, *19*, 4557. (j) Zawadzki, M.; Okal, J. *Mater. Res. Bull.* **2008**, *43*, 3111. (k) Boutros, M.; Denicourt-Nowicki, A.; Roucoux, A.; Gengembre, L.; Beaunier, P.; Gedeon, A.; Launay, F. *Chem. Commun.* **2008**, 2920. (l) Xing, R.; Liu, Y.; Wu, H.; Li, X.; He, M.; P., W. *Chem. Commun.* **2008**, 6297. (m) Elmoula, M. A.; Panaitescu, E.; Phan, M.; Yin, D.; Richter, C.; Lewis, L. H.; Menon, L. *J. Mater. Chem.* **2009**, *19*, 4483. (n) Xie, Y.; Ding, K.; Liu, Z.; Tao, R.; Sun, Z.; Zhang, H.; An, G. *J. Am. Chem. Soc.* **2009**, *131*, 6648. (o) Besson, E.; Mehdi, A.; Reye, C.; Corriu, R. J. P. *J. Mater. Chem.* **2009**, *19*, 4746. (p) Lin, Z.; Chu, H.; Shen, Y.; Wei, L.; Liu, H.; Li, Y. *Chem. Commun.* **2009**, 7167. (q) Zahmakiran, M.; Özkar, S. *Langmuir* **2009**, *25*, 2667. (r) Zahmakiran, M.; Özkar, S. *J. Am. Chem. Soc.* **2010**, *132*, 6541. In addition, the catalysts elsewhere[26−29] were also prepared in contact with solution.

(19) "Weakly ligated/labile ligand" nanoparticles are simply nanoparticles with ideally 100% removable or replaceable ligands prepared using only the desired reactants (or solvent) for the catalytic reaction at hand. Related concepts, such as putatively "solvent-only" stabilized nanoparticles, are discussed in: (a) Ott, L. S.; Finke, R. G. *Inorg. Chem.* **2006**, *45*, 8382. A recent review has also been published[3h] detailing nanoparticle stabilization and the use of anion free metal precursors that, in principle, can generate such "weakly ligated/labile ligand" or "solvent only" stabilized nanoparticles. See footnote 41 in ref 14 for related work on putatively "naked nanoparticles".

(20) Our own efforts to date on the "weakly ligated/labile ligand" nanoparticle concept are reported in: (a) Özkar, S.; Finke, R. G. *J. Am. Chem. Soc.* **2005**, *127*, 4800. (b) Bayram, E.; Zahmakiran, M.; Özkar, S.; Finke, R. G. *Langmuir* **2010**, *26*, 12455.

(21) Bell, A. T. *Science* **2003**, *299*, 1688.

(22) Lee, I.; Delbecq, F.; Morales, R.; Albiter, M. A.; Zaera, F. *Nat. Mater.* **2009**, *8*, 132.

(23) Joo, S. H.; Park, J. Y.; Tsung, C.-H.; Yamada, Y.; Yang, P.; Somorjai, G. A. *Nat. Mater.* **2009**, *8*, 126.

(24) (a) Thomas, J. M.; Johnson, B. F. G.; Raja, R.; Sankar, G.; Midgley, P. A. *Acc. Chem. Res.* **2003**, *36*, 20. (b) Alayoglu, S.; Nilekar, A. U.; Mavrikakis, M.; Eichhorn, B. *Nat. Mater.* **2008**, *7*, 333.

(25) Che, M.; Bennett, C. O. *Adv. Catal.* **1989**, *36*, 55.

(26) Two hypothesized,[27,28] but not experimentally tested, mechanisms have been put forth in the supported-nanoparticle heterogeneous catalyst formation in contact with solution literature. Marre et al.[27] studied the formation of $Cu(0)_n/(SiO_2)_n$ (silica spheres) starting from $Cu(hfac)_2 \cdot H_2O$ (where hfac = hexafluoroacetylacetonate) in supercritical CO_2/alcohol/H_2 mixtures. They propose that the $Cu(0)_n/(SiO_2)_n$ products are formed via a mechanism consisting of an initial homogeneous nucleation, followed by deposition, and subsequent coagulation and coalescence. Unfortunately, the physical model used to test their hypothesis is not based on rigorous chemical reactions (as is required in chemical kinetics), so that the words used to describe those processes (e.g., homogeneous nucleation, coagulation, and so on) do not have a sound, reliable mechanistic basis, an insidious nomenclature problem that leads to considerable mechanistic confusion as addressed elsewhere.[26a] Furthermore, no alternative mechanisms were disproved for that specific $Cu(0)_n/(SiO_2)_n$ system, as discussed further in our review.[30] Despite these issues, it is noteworthy the data herein (albeit for a different, Ir system) are consistent with the general mechanism proposed by Marre et al. for their versus Cu system. Rossi and coworkers[29] have also briefly reported Pd^{2+}/SiO_2 to $Pd(0)_n/SiO_2$ supported-nanoparticle formation kinetics in contact with solution, using the cyclohexene reporter reaction method shown in Scheme 2. Unfortunately, the needed stirring rate and $[cyclohexene]^0$-dependent controls were not performed, making it unclear whether the $Pd(0)_n$ supported-nanoparticle formation kinetics are being faithfully monitored;[4,14] furthermore, no mechanism was proposed for the observed kinetics. Additional evidence consistent with a solution-based mechanism comes from the groups of Chaudret[26b] and Corain[26c,d] who demonstrated that solvents were needed for supported-nanoparticle products to form in their system. Wang et al.[28] studied the formation of a $Pt(0)_n$/carbon nanotube (CNT) catalyst starting from H_2PtCl_6 in ethylene glycol and in the presence of sodium dodecylsulfate. In contrast with Marre et al., they concluded that the $Pt(0)_n$/CNT catalyst formation occurred via heterogeneous nucleation on the CNT surface, followed by autocatalytic

surface growth[4] effectively depleting the Pt^{4+} monomers in solution. Other literature, by Muramatsu and co-workers,[26e,f] further asserts that nucleation must occur on the surface at solid−liquid interfaces, for example, in the presence of catalyst support materials. Overall, this brief survey of the literature makes apparent that definitive work on the mechanisms of nanoparticle formation in contact with solution is not available from the prior literature. (a) Finney, E. E.; Finke, R. G. *Chem. Mater.* **2009**, *21*, 4692. (b) Hulea, V.; Brunel, D.; Galarneau, A.; Philippot, K.; Chaudret, B.; Kooyman, P. J.; Fajula, F. *Microporous Mesoporous Mater.* **2005**, *79*, 185. (c) Artuso, F.; D'Archivio, A. A.; Lora, S.; Jerabek, K.; Kralik, M.; Corain, B. *Chem.-Eur. J.* **2003**, *9*, 5292. (d) Corain, B.; Jerabek, K.; Centomo, P.; Canton, P. *Angew. Chem., Int. Ed.* **2004**, *43*, 959. (e) Takahashi, H.; Sunagawa, Y.; Myagmarja, S.; Muramatsu, A. *Catal. Surv. Asia* **2005**, 9. (f) Sunagawa, Y.; Yamamoto, K.; Takahashi, H.; Muramatsu, A. *Catal. Today* **2008**, *132*, 81.

(27) (a) Marre, S.; Cansell, F.; Aymonier, C. *Nanotechnology* **2006**, *17*, 4594. (b) Marre, S.; Erriguible, A.; Perdomo, A.; Cansell, F.; Marias, F.; Aymonier, C. *J. Phys. Chem. C* **2009**, *113*, 5096.

(28) Wang, Y.; Xu, X.; Tian, Z.; Zong, Y.; Cheng, H.; Lin, C. *Chem.-Eur. J.* **2006**, *12*, 2542.

(29) Rossi, L. M.; Nangoi, I. M.; Costa, N. J. S. *Inorg. Chem.* **2009**, *48*, 4640.

(30) Mondloch, J. E.; Bayram, E.; Finke, R. G., manuscript in preparation. ("A Review of the Kinetics and Mechanisms of Formation of Supported-Nanoparticle Heterogeneous Catalysts" (tentative title))

(31) Our prior work[14] is certainly not the first example of a well-characterized organometallic precatalyst. Extensive examples of well-characterized organometallic precatalysts can be found in: (i) Zakharov, V. A.; Yermakov, Y. I. *Catal. Rev.-Sci. Eng.* **1979**, *19*, 67.(ii) *Modern Surface Organometallic Chemistry*; Basset, J.-M., Psaro, R., Roberto, D., Ugo, R., Eds.; Wiley-VCH: Weinheim, 2009. However, ours is the first study that starts from a well-characterized speciation-controlled supported organometallic precatalyst and focuses on supported-nanoparticle heterogeneous catalyst formation in contact with solution, and which contains the necessary kinetic data to rule out alternative mechanisms en route to a kinetically supported proposed mechanism.

(32) The eight prototype criteria previously developed[14] are (i) a compositionally and structurally well-defined supported precatalyst (accomplished previously via inductively coupled plasma optical emission spectroscopy, CO/IR trapping experiments, as well as X-ray absorbance fine structure (XAFS) spectroscopy[14]); (ii) a system in contact with solution and formed under low temperature conditions; and (iii) a system where a balanced stoichiometry of the supported-nanoparticle formation reaction is established (e.g., Scheme 1, and as previously confirmed elsewhere[14]), leading to a well-defined $Ir(0)_{\sim 900}/\gamma\text{-}Al_2O_3$ supported-nanoparticle heterogeneous catalyst (confirmed for the present system by transmission electron microscopy (TEM) and XAFS[14]). In addition, a prototype system should: (iv) yield an active and long-lived catalyst, and hence (v) provide a system where the initial kinetic and mechanistic studies of the in situ catalyst formation are worth the effort. The prototype system should also yield (vi) reproducible and quantitative kinetic data so that quantitative conclusions and mechanistic insights can be drawn; and ideally (vii) comparison to a kinetically and mechanistically well-studied nanoparticle formation system in solution should also be possible for any insights that comparison might allow.[4,34,45] Last, once that prototype system is in hand, one would also like to (viii) systematically vary key synthetic variables such as the support, solvent, and metal precursor to reveal their affects on supported-nanoparticle formation in contact with solution.

(33) Lyon, D. K. Ph.D. Dissertation, University of Oregon, September 1990.

(34) (a) Lin, Y.; Finke, R. G. *J. Am. Chem. Soc.* **1994**, *116*, 8335. (b) Lin, Y.; Finke, R. G. *Inorg. Chem.* **1994**, *33*, 4891.

(35) The mechanism in Scheme 3 predicts that k_{1obs} and k_{2obs} should be constant as a function of the $Ir(1,5\text{-COD})Cl/\gamma\text{-}Al_2O_3$ wt %, a result that we confirmed. To probe the $[\gamma\text{-}Al_2O_3]_{sus}$ dependence on k_{1obs} and k_{2obs}, it is best to study this as a constant initial $Ir(1,5\text{-COD})Cl/\gamma\text{-}Al_2O_3$ wt % as was done in the present studies.

(36) The details on the typically observed error limits in k_1 of $\pm 10^{1.2}$ h^{-1} derived over a >7 year period from data obtained from multiple investigations, all for the $P_2W_{15}Nb_3O_{62}^{9-}$ polyoxoanion-stabilized $Ir(0)_{\sim 300}$ nanoparticle system, have previously been described: Widegren, J. A.; Bennett, M. A.; Finke, R. G. *J. Am. Chem. Soc.* **2003**, *125*, 10301 (specifically p 10304). Briefly, k_1 has been shown to be sensitive to water, acetone impurities, precursor purity, and amount of any $Ir(1,5\text{-COD})^+$ unbound to the $P_2W_{15}Nb_3O_{62}^{9-}$ polyoxoanion.[4,34,45] While significantly less data have been collected for the prototype $Ir(1,5\text{-COD})Cl/\gamma\text{-}Al_2O_3$ to $Ir(0)_{\sim 900}/\gamma\text{-}Al_2O_3$ system, the observed error limits to data are $\sim\pm 10^1$ h^{-1} for k_1[14] and are also expected to be sensitive to water, acetone, and precursor purity, and the amount of any excess or otherwise unbound $Ir(1,5\text{-COD})^+$. Another relevant point is that other k_1 nucleation rate constants, given elsewhere[6−8] (e.g., for a four-step mechanism for nanoparticle nucleation, autocatalytic surface growth, bimolecular agglomeration, and autocatalytic agglomeration), have been shown to vary by $\sim\pm 10^4$.

(37) A datum point at 0.163 M $\gamma\text{-}Al_2O_3$ (i.e., without any additional $\gamma\text{-}Al_2O_3$) is available, with the following observed rate constants: $k_{1obs} = 1.5(1) \times 10^{-3}\ h^{-1}$ and $k_{2obs} = 1.6(2) \times 10^4\ h^{-1}\ M^{-1}$.[14] However, this point was not, and should not, be coplotted with the data in Figures 2 and 3 because that system is not equilibrated with any additional $[\gamma\text{-}Al_2O_3]_{sus}$. Such equilibration steps, and the order(s) of addition of the reagents, have been shown to be experimentally important variables in the $Ir(1,5\text{-COD})Cl/\gamma\text{-}Al_2O_3$ precatalyst preparation and subsequent supported-nanoparticle heterogeneous catalyst formation kinetics.[14] Hence, it follows that only samples prepared under the same synthetic conditions should be (and were) plotted in Figures 2 and 3.

(38) In neat cyclohexane, the UV−vis spectrum of the filtered solution (Figure S3 in the Supporting Information) reveals that no $Ir(1,5\text{-COD})Cl(solvent)$ is present in solution. However, in acetone, two metal-to-ligand charge transfer bands are present from 340 to 540 nm (detailed in the Supporting Information), data consistent with the presence of a square planar Ir(I) complex in acetone.[39]

(39) Epstein, R. A.; Geoffroy, G. L.; Keeney, M. E.; Mason, W. R. *Inorg. Chem.* **1970**, *18*, 478.

(40) The acetone-dependent data above ~1.75 M acetone show saturation behavior, consistent with the solution-based mechanism. However, those data are convoluted due to competing H_2 gas-to-solution mass-transfer limitations (MTLs) due to the lower solubility of H_2 in the mixed cyclohexane/acetone solvent system versus that in acetone. The MTLs were revealed by stirring the supported-nanoparticle heterogeneous catalyst formation reactions (i.e., those above ~1.75 M acetone) at 1000 rpm. That 40% increase in stirring rate yielded a 40% increase in the H_2 uptake rate, $-d[H_2]/dt$. The observed H_2 gas-to-solution MTL largely affect k_{2obs} as it correlates with the H_2 uptake during nanoparticle growth (i.e., post the induction period), but has a minimal affect on k_{1obs} (i.e., the nucleation step uses little H_2 and, therefore, is not MTL under these conditions).[4]

(41) Dalla Betta, R. A.; Boudart, M. *International Congress on Catalysis (5th)*; North Holland: Palm Beach, FL, 1972; Vol. 5, p 1329.

(42) One relevant question is "approximately how large, on average, are the $Ir(0)_n$ nanoparticles when they are captured by the $\gamma\text{-}Al_2O_3$ support?" This can be estimated using our previously obtained[14] cyclooctane evolution kinetic data. Those data reveal that at the end of the induction period (approximately 20−30 min), only 2.1% or 4.9% of the $Ir(1,5\text{-COD})Cl/\gamma\text{-}Al_2O_3$ precatalyst has evolved into $Ir(0)_n$. Because nucleation and growth are separated in time, we can estimate from the average $Ir(0)_{\sim 900}$ supported-nanoparticle product that, on average, $Ir(0)_{\sim 19}$ to $Ir(0)_{\sim 44}$ nanoparticles are captured by the $\gamma\text{-}Al_2O_3$. That is, approximately 0.8−1.1 nm nanoparticles are formed during the nucleation step, which are then captured by the $\gamma\text{-}Al_2O_3$ and then grow (via autocatalytic surface growth) to the observed, on average 2.9 nm $Ir(0)_{\sim 900}$ nanoparticles on the $\gamma\text{-}Al_2O_3$.

(43) Watzky, M. A.; Finney, E. E.; Finke, R. G. *J. Am. Chem. Soc.* **2008**, *130*, 11959.

(44) Ott, L. S.; Finke, R. G. *J. Nanosci. Nanotechnol.* **2008**, *8*, 1551.

(45) Widegren, J. A.; Aiken, J. D., III; Özkar, S.; Finke, R. G. *Chem. Mater.* **2001**, *13*, 312.

(46) Aiken, J. D., III; Lin, Y.; Finke, R. G. *J. Mol. Catal. A: Chem.* **1996**, *114*, 29.

(47) http://www.city-data.com/city/Fort-Collins-Colorado.html (accessed Nov 7, 2010).

(48) An important control experiment, using 500 °C partially dehydroxylated γ-Al_2O_3,[49] ensured that the γ-Al_2O_3 degree of hydroxylation/water content was controlled for the kinetic experiments herein. The average of two supported-nanoparticle heterogeneous catalyst formation kinetic experiments, using 500 °C partially dehydroxylated 2.0 wt % Ir(1,5-COD)Cl/γ-Al_2O_3, yielded a k_1 rate constant of $1.3(2) \times 10^{-3}$ h^{-1} and a k_2 rate constant of $1.6(2) \times 10^{4}$ h^{-1} M^{-1} (vs the 160 °C thermally treated γ-Al_2O_3 k_1 and k_2 rate constants of $1.5(1.1) \times 10^{-3}$ h^{-1} and $1.6(2) \times 10^{4}$ h^{-1} M^{-1}, respectively). Hence, there is no difference in the k_1 and k_2 rate constants for the 160 and 500 °C thermally treated γ-Al_2O_3 samples.

(49) Partially dehydroxylated γ-Al_2O_3 was made following the procedure of: Lobo-Lapidus, R. J.; McCall, M. J.; Lanuza, M.; Tonnesen, S.; Bare, S. R.; Gates, B. C. *J. Phys. Chem. C* **2008**, *112*, 3383. Specifically, the γ-Al_2O_3 powder was calcinced for 4 h at 500 °C in flowing O_2 at 1 atm, followed by evacuation under vacuum for 24 h.

(50) Motulsky, H.; Chrsitopoulos, A. *Fitting Models to Biological Data Using Linear and Nonlinear Regression*; Oxford University Press: New York, 2004.

(51) We thank a reviewer for arguing for the need to use weighted nonlinear regression to accurately fit the k_{1obs} and k_{2obs} versus $[\gamma\text{-}Al_2O_3]_{sus}$ and [acetone] data.